ADAREP: PLUG-AND-PLAY ACCELERATION FOR WORLD MODEL PREDICTIVE CONTROL USING ADAPTIVE RE-PLANNING

Anonymous authors

000

001

002

003

004

006

012 013

014

016

017

018

019

021

024

025

026

027

028

031

033

034

037

038

040

041

042 043

044

046

047

048

051

052

Paper under double-blind review

ABSTRACT

We investigate the integration of model predictive control (MPC) with world models for robotic control tasks. Existing MPC solvers often replan at every step or after very few steps, primarily to mitigate the accumulation of world model prediction errors. However, such frequent replanning incurs substantial computational costs – especially when using large, complex world models. In this work, we theoretically characterize the fundamental trade-off between computational efficiency and control performance in MPC. Our analysis reveals how replanning frequency, model prediction error, and local dynamics sensitivity jointly influence MPC performance, as captured by regret bounds. Based on the analysis, we propose ADAREP, a novel adaptive replanning mechanism for MPC that dynamically modulates the replanning frequency based on online estimates of world model prediction error and local dynamics sensitivity. ADAREP is training-free, plug-andplay, and compatible with various world models and MPC solvers. Experiments on the VP2 simulation benchmark across diverse tasks, as well as real-world robotic tasks including door opening and T-block pushing, show that ADAREP achieves substantial reductions in computation, over 80–90% in the real-world settings while maintaining or improving task success rates. Code will be made public.

1 Introduction

This paper studies model predictive control (MPC) combined with learned world models for various robotic control tasks (Ding et al., 2024; Campbell et al., 2023; Wu et al., 2024; Tian et al., 2023a; Zhao et al., 2024). Typically, a predictive world model is first trained to forecast future robot and environment states (*e.g.*, images) based on historical states and robot actions. MPC solvers, such as the Cross-Entropy Method (CEM) or Model Predictive Path Integral control (MPPI), then sample multiple action sequences and query the world model to predict their outcomes. Action sequences that are more likely to achieve the specified goals – based on the predicted future states – are selected for execution (De Boer et al., 2005; Anderson & Moore, 2007). Fueled by the powerful pretrained generative models Ho et al. (2020); Rombach et al. (2022), MPC using these generative world models has been applied to a variety of robotic tasks, including manipulation and navigation Du et al. (2023); Yang et al. (2023); Wang et al. (2024).

Despite their effectiveness, MPC with learned world models can suffer from computational inefficiency. As illustrated in Figure 1, to mitigate cumulative prediction errors, many MPC solvers avoid executing full action plans and instead replan at every step or after only a few steps. This frequent replanning greatly increases the number of world model queries, leading to higher computational cost and reduced control frequency due to delays. The use of large, complex world models further exacerbates this issue.

To this end, we propose ADAREP, a novel adaptive replanning mechanism for MPC. Our **key idea** is to dynamically modulate the replanning frequency in MPC. We start by theoretically characterizing the fundamental trade-off between computation efficiency and control performance in MPC. Our analysis shows how the MPC regret bounds, which capture the performance, can be jointly affected by replanning frequency, world model prediction error, and local dynamic sensitivity. We therefore design an algorithm to adjust the replanning frequency based on online estimates of world model pre-

056

058

060

061 062

063

064

065

066

067

068

069

071

072

073

074

075

076

077

079 080

081

082

084

085

087

090

092 093

094

096

098

099

100 101

102

103

104 105

106

107

Figure 1: An illustration of the computational efficiency—control performance trade-off in MPC and our ADAREP: Traditional MPC solvers replan frequently to curb cumulative world-model prediction error, driving up computation. By contrast, ADAREP adjusts replanning frequency on-the-fly using online estimates of prediction error and local dynamics sensitivity, cutting computation while preserving control performance.

diction error and local dynamics sensitivity. ADAREP is training-free, plug-and-play, and compatible with various world models and MPC solvers. An overview of ADAREP can be found in Figure 1.

We conduct an extensive evaluation of our method on both simulated and real-world robotic control, ranging from the diverse tasks in VP2 simulation benchmark to real-world door opening and T-block pushing. Overall, when combined with a collection of world models and MPC solvers, ADAREP demonstrates a substantial reduction of computation – over 80-90% – as measured by number of function evaluations (NFEs), while maintaining the task success rate. Our additional analysis further reveals the control scenarios where ADAREP suits better.

To sum up, our contributions are threefold:

- We provide a rigorous regret analysis of MPC replanning strategies, offering theoretical insights into the computation efficiency-control performance trade-off.
- We develop ADAREP, a practical and efficient plug-and-play adaptive replanning algorithm for MPC, designed to enhance computational efficiency while maintaining robust control performance; unlike prior methods that replan every step, ADAREP decides when to replan.
- We present experimental validation in both simulated and real-world robotic manipulation tasks, demonstrating the effectiveness and robustness of our proposed adaptive approach compared to canonical MPC solvers.

2 Preliminaries

Model Predictive Control. We begin by outlining the general formulation for finite-horizon, discrete-time optimal control, which forms the basis for our discussion. We consider problems characterized by potentially time-varying costs, dynamics, and constraints. The objective is to determine state and control trajectories, denoted by $x_{0:T}$ and $u_{0:T-1}$ respectively, that solve the following optimization problem:

$$\min_{x_{0:T}, u_{0:T-1}} \sum_{t=0}^{T-1} f_t(x_t, u_t; \xi_t^*) + F_T(x_T; \xi_T^*)
\text{s.t. } x_{t+1} = g_t(x_t, u_t; \xi_t^*), \qquad \forall 0 \le t < T,
s_t(x_t, u_t; \xi_t^*) \le 0, \qquad \forall 0 \le t < T,
x_0 = x(0).$$
(1)

Here, $x_t \in \mathbb{R}^n$ represents the system *state* at time t, and $u_t \in \mathbb{R}^m$ is the *control input* or *action*. The function f_t denotes the time-varying *stage cost*, g_t represents the time-varying system *dynamics*, and s_t encapsulates the time-varying *constraints*. Crucially, these functions are parameterized by ξ_t^* ,

representing unknown ground-truth parameters governing the system's behavior at time t. F_T is a terminal cost function, parameterized by ξ_T^* , applied to the final state x_T . The initial state is given by x(0).

A widely adopted approach for addressing such problems, particularly in online settings where future parameters ξ_t^* are unknown, is *Model Predictive Control (MPC)*. Solving the full-horizon problem equation 1 directly is often impractical, even if an estimate ξ_t of the true parameters ξ_t^* is available. Two primary challenges arise:

- 1. **Computational Complexity:** Solving the large-scale optimization problem equation 1 can be computationally prohibitive, especially for long horizons *T*.
- 2. **Model Mismatch & Error Accumulation:** Using an imperfect model (parameterized by ξ_t instead of ξ_t^*) over a long horizon can lead to the accumulation of prediction errors, potentially resulting in significant performance degradation or constraint violations.

To mitigate these issues, MPC employs a *receding horizon* strategy. At each time step t, given the current state x_t and potentially updated parameter estimates $\xi_{t:\min(t+k,T)-1}$, MPC solves a *Finite-Time Optimal Control Problem (FTOCP)* over a shorter prediction horizon k.

Definition 2.1 (FTOCP). The Finite-Time Optimal Control Problem (FTOCP) over the horizon $[t_1, t_2]$, initialized at state z, using parameters $\xi_{t_1:t_2-1}$, terminal parameter ζ_{t_2} , and terminal cost function $F(\cdot; \cdot)$, seeks to find the minimum cost:

$$\iota_{t_{1}}^{t_{2}}(z, \xi_{t_{1}:t_{2}-1}, \zeta_{t_{2}}; F) := \min_{y_{t_{1}:t_{2}}, v_{t_{1}:t_{2}-1}} \sum_{t=t_{1}}^{t_{2}-1} f_{t}(y_{t}, v_{t}; \xi_{t}) + F(y_{t_{2}}; \zeta_{t_{2}})$$

$$s.t. \ y_{t+1} = g_{t}(y_{t}, v_{t}; \xi_{t}), \qquad \forall t_{1} \leq t < t_{2},$$

$$s_{t}(y_{t}, v_{t}; \xi_{t}) \leq 0, \qquad \forall t_{1} \leq t < t_{2},$$

$$y_{t+1} = z.$$

$$(2)$$

 $Let \ \psi_{t_1}^{t_2}(z,\xi_{t_1:t_2-1},\zeta_{t_2};F) \ denote \ a \ corresponding \ optimal \ trajectory \ solution \ (y_{t_1:t_2},v_{t_1:t_2-1}).$

The FTOCP equation 2 is solved at the current time t over the horizon $[t, \min(t+k, T)]$ using the current state x_t as the initial state z. From the resulting optimal control sequence $v_{t:\min(t+k,T)-1}$, only the first control action, $u_t = v_t$, is applied to the actual system dynamics $g_t(\cdot, \cdot; \xi_t^*)$. The system transitions to the next state x_{t+1} , and the process repeats at time t+1. A typical implementation is described in MPC $_k^1$ (Algorithm 2).

Measuring Control Performance of MPC. We evaluate online control algorithms (ALG) by comparing their executed trajectories against the offline optimal trajectory (OPT), which assumes perfect foresight of ground-truth parameters $\xi_{0:T}^*$.

Definition 2.2 (Trajectories). Given initial state x_0 and parameters $\xi_{0:T}^*$:

- Executed Trajectory (obtained from ALG): $x_0 \xrightarrow{u_0} \cdots \xrightarrow{u_{T-1}} x_T$, where u_t is chosen by ALG and $x_{t+1} = g_t(x_t, u_t; \xi_t^*)$.
- Offline Optimal Trajectory (OPT): $x_0^* \xrightarrow{u_0^*} \cdots \xrightarrow{u_{T-1}^*} x_T^*$, solving equation 1 with known $\xi_{0:T}^*$.

Our primary performance metric is *dynamic regret* (Li et al., 2020; Gandhi et al., 2021; Dogan et al., 2023; Goel et al., 2019; Fiacco & Ishizuka, 1990), quantifying the cumulative cost difference between the executed and optimal trajectories due to the online nature of the algorithm:

$$Regret(ALG) := cost(ALG) - cost(OPT), \qquad (3)$$

where $cost(\cdot)$ is the total trajectory cost calculated using true parameters ξ_t^* :

$$\operatorname{cost}(\mathsf{ALG}) \coloneqq \sum_{t=0}^{T-1} f_t(x_t, u_t; \xi_t^*) + F_T(x_T; \xi_T^*) \quad \operatorname{cost}(\mathsf{OPT}) \coloneqq \sum_{t=0}^{T-1} f_t(x_t^*, u_t^*; \xi_t^*) + F_T(x_T^*; \xi_T^*) \;.$$

Measuring Computation Efficiency of MPC. To assess computational efficiency, especially crucial when using learned world models, we choose *Number of Function Evaluations (NFEs)*: The

total number of predictive world model queries made by the MPC solver (e.g., CEM, MPPI) during one episode (t=0 to T). NFE directly reflects the computation cost and potential for acceleration. Using NFE or similar query counts as a measure of computational efficiency is common practice in related fields, including optimization (ten Eikelder & van Amerongen, 2023), generative modeling (Prasad et al., 2024), and large language model planning (Sun et al., 2023).

3 METHODOLOGY

The core objective of our methodology is to enhance the computational efficiency of MPC when using learned world models, specifically by minimizing the Number of Function Evaluations (NFE), without significantly compromising control performance, as measured by dynamic regret. More specifically, we aim to minimize the NFE conditioned on the overall regret is no more than $(\varepsilon + \text{Regret}(\text{MPC}_k^1))$ We achieve this by developing adaptive replanning strategies and analyzing their theoretical properties and practical effectiveness.

3.1 THEORETICAL ANALYSIS

Standard Model Predictive Control can be computationally demanding. This is particularly true when employing complex predictive models (e.g., learned world models) and sampling-based optimizers (e.g., Model Predictive Path Integral control (MPPI)(Williams et al., 2017), Cross-Entropy Method (CEM)(De Boer et al., 2005)), which may require hundreds or thousands of model queries per control step.

Natural approaches to accelerate the planning process involve reducing the replanning frequency. Two such strategies are considered:

- MPC $_k^m$: Execute a fixed number, $m \ge 1$, of actions from the computed plan before replanning (Algorithm 3).
- MPC_{k,\epsilon}: Replan only when the system state deviates significantly (by more than a threshold ϵ) from the previously planned trajectory (Algorithm 4).

Intuitively, reducing the replanning frequency may degrade control performance compared to standard MPC_k^1 . We aim to characterize this trade-off between computational savings and performance, measured by dynamic regret, both theoretically and empirically.

Our theoretical analysis builds upon perturbation analysis techniques (Shin et al., 2020; Lin et al., 2021; Shin & Zavala, 2021; Xu & Anitescu, 2019; Na & Anitescu, 2022) and adapts the 3-step analytical pipeline proposed by Lin et al. (2022). Detailed derivations are deferred to Appendices C and D, while the main theoretical results on dynamic regret are summarized in Table 1.

Table 1: Overview of theoretical regret bounds. Here, $L = \max_{0 \le t < T} L_t$ and $L_* = \max_{0 \le t \le T} \max_{0 \le i \le m-1} \prod_{s=t}^{t+i} L_s$ characterize the sensitivity (Lipschitz constants) of the dynamics over single and multiple steps, respectively. E represent cumulative prediction errors of the underlying model. Note that when m=1 or $\epsilon=0$, our results recover (Lin et al., 2022). NFEs decreases as m, ϵ, α_L and α_δ increases. Full table on the characterization of NFE details can be found in Table 2.

| Algorithm Reference | | Regret Bound |
|---------------------|-------------------|---|
| MPC^1_k | Lin et al. (2022) | $O\left(\sqrt{L^2 \mathrm{cost}(OPT) \cdot E} + L^2 E\right)$ |
| MPC^m_k | Theorem C.4 | $O\left(\sqrt{mL_*^2\mathrm{cost}(OPT)\cdot E} + mL_*^2E\right)$ |
| $MPC_{k,\epsilon}$ | Theorem C.6 | $O\left(\sqrt{L^2 \text{cost}(OPT) \cdot (E + \epsilon E + \epsilon^2 T)} + L^2(E + \epsilon E + \epsilon^2 T)\right)$ |
| MPC_{AR} | Theorem C.7 | $O\left(\sqrt{\cos(OPT)(L^2E + \frac{\epsilon_0}{\alpha_L^2}(\epsilon_0 + \frac{1}{\alpha_\delta})T)} + L^2E + \frac{\epsilon_0}{\alpha_L^2}(\epsilon_0 + \frac{1}{\alpha_\delta})T\right)$ |

Our theoretical analysis reveals that the major additional regret in MPC_{k, ϵ} is $\epsilon L^2E + \epsilon^2L^2T$, highlighting the tradeoff between computational efficiency and control performance. This suggests choosing more aggressive ϵ when both prediction error E and dynamics sensitivity L are small.

Theoretically, we can set $\epsilon \propto \exp(-\alpha_L L) \cdot \exp(-\alpha_\delta E)$, leveraging the exponential decay property $x \exp(-\alpha x) \leq \frac{1}{e\alpha}$ to control regret through parameter α .

However, fixed strategies are suboptimal in practice since both prediction error and dynamics sensitivity vary significantly over time. We therefore introduce MPC $_{AR}$ (Algorithm 5), which adaptively adjusts the threshold online, as detailed in the following subsection.

3.2 ADAREP: AN ADAPTIVE REPLANNING MECHANISM

The core idea of ADAREP is to dynamically adjust the replanning strategy based on real-time performance metrics, specifically model prediction accuracy and local dynamics sensitivity. The goal is to replan less frequently (saving computation) when the model performs well and the system behaves predictably, but increase replanning frequency when prediction errors rise or the system exhibits higher sensitivity. The detailed procedure is implemented in Algorithm 1 and Algorithm 5.

The adaptation relies on metrics computed at each time step. Let $(y_{t:...}, v_{t:...})$ be the plan computed at time step t. After applying the first action $u_t = v_t$ and observing the actual next state x_{t+1} resulting from the true dynamics $g_t(\cdot, \cdot; \xi_t^*)$, we calculate:

1. **Prediction Error:** The deviation between the observed state and the state predicted by the model $g_t(\cdot,\cdot;\xi_t)$ used for planning (denoted y_{t+1} in the plan starting from x_t).

$$\delta_{t+1}^o = \|x_{t+1} - y_{t+1}\| , \qquad (4)$$

where $y_{t+1} = g_t(x_t, u_t; \xi_t)$ according to the internal model.

2. **Local Dynamics Sensitivity Estimator:** An estimate of how much the state changes relative to the control input magnitude, which provides an empirical measure of the system's local sensitivity.

$$\widehat{L}_t = \frac{\|x_{t+1} - x_t\|}{\|u_t\|} \,, \tag{5}$$

A higher \widehat{L}_t suggests greater state change per unit control, indicating higher local sensitivity.

3. **Threshold Update:** Based on the estimators, we update the threshold inversely to the estimators. Here we simply apply exponential descay.

$$\epsilon_t = \epsilon_0 \cdot \exp\left(-\alpha_L \hat{L}_t\right) \cdot \exp\left(-\alpha_\delta \delta_t^o\right).$$
 (6)

Algorithm 1 ADAREP: Adaptive Re-Planning Threshold Update (theoretical version)

Require: action u_t , prediction y_{t+1} , base threshold ϵ_t

- 1: Calculate prediction error δ_t^o using Equation (4)
- 2: Estimate local dynamics sensitivity \hat{L}_t by Equation (5)
- 3: Update the threshold ϵ_t by Equation (6)

We also provide theoretical regret analysis for this algorithm in Theorem C.7, which reveals how we can manipulate the additional regret by simply setting different values of ϵ_0 , α_L , and α_δ , with no reliance on L or E, which is not supported by non-adaptive methods like MPC_k^m or $\mathsf{MPC}_{k,\epsilon}^n$.

Implementation Details Practical implementation of our algorithm involves several key details:

- 1. **Sliding Window:** The estimators calculated by Equation (4) and Equation (5) are quite noisy. To achieve more stable update, we apply sliding window to stabilize the adaptation against noisy single-step measurements. Our sensitive analysis in Section 4.3 demonstrate that sliding window method are crucial for practical implementations.
- 2. **State Distance Calculation:** The method for calculating distances, particularly the prediction error $\delta_{t+1}^o = \|x_{t+1} y_{t+1}\|_2$ (Equation (4)), depends on the nature of the predictive world model:
 - For **state-based world models** that directly output predicted state vectors, we compute the L2-norm $(\|\cdot\|_2)$ between the actual and predicted state vectors.

• For vision-based world models that output predicted images, calculating distances directly in pixel space is often ineffective. Instead, we first extract semantic features from both the actual observed image $(I(x_{t+1}))$ and the predicted image $(I(y_{t+1}))$ using a pre-trained feature extractor, such as DINO (Caron et al., 2021). Let $\phi(\cdot)$ denote this feature extraction function. The prediction error is then computed in the feature space:

 $\delta_{t+1}^o = \|\phi(I(x_{t+1})) - \phi(I(y_{t+1}))\|_2 . \tag{7}$

3. **Hyper-parameters Tuning:** Our tuning is an upfront and efficient process as it builds upon the baseline. A practitioner can start with a reasonable fixed threshold ϵ and then simply tune α_L and α_δ , which control the adaptation's sensitivity. Note that we do not need to tune the algorithm again if we switch the MPC planners (eg. MPPI,CEM).

Finally we remark that ADAREP is a training-free, plug-and-play module that can seamlessly be adapted to any world models and MPC planners. It can be adapted to **any** tasks that standard MPC $_k^1$ can handle.

4 EXPERIMENTS

4.1 Experiment settings

 Our experiments are designed to address the following key questions regarding our proposed adaptive replanning algorithm:

1. **Efficiency and Performance:** Does our proposed algorithm significantly accelerate the planning process compared to canonical MPC solvers while maintaining comparable or achieving even better task performance? (Figure 2)

2. **Generalization:** Does the adaptive replanning mechanism generalize effectively across different predictive world models and diverse manipulation tasks within the simulated environment? (Figure 2)

3. **Real-World Applicability:** Can the benefits observed in simulation translate to challenging real-world robotic planning scenarios using learned world models? (Figure 3)

Simulated Experiments. We conduct simulated experiments using the VP2 benchmark (Tian et al., 2023b), a control-centric benchmark designed for evaluating video prediction models in manipulation tasks. This allows us to assess our algorithm's effectiveness and adaptability across various world models and tasks in a controlled setting. VP2 utilizes the RoboDesk simulation environment (Kannan et al., 2021) and provides pre-trained predictive world models relevant to this environment.

The RoboDesk environment features a Franka Emika Panda robot arm situated before a desk with various objects. We evaluate on the following 7 tasks defined within RoboDesk: pushing buttons (red, green, blue), opening a slide, opening a drawer, and pushing blocks (upright, flat) off the table.

We test our adaptive replanning approach with two distinct open-source video predictive world models provided by the VP2 benchmark: SVG (Villegas et al., 2019) and Struct-VRNN (Minderer et al., 2019). These models represent different architectural choices for video prediction. Here we compare our adaptive method MPC $_{AR}$ against standard MPC $_k$ and other non-adaptive method MPC $_k$ and MPC $_k$.

Real-World Experiments. To assess performance beyond simulation, we conduct real-world experiments with a Franka Emika Panda robotic arm, as detailed in Appendix E.2. we utilize state-based world models trained as described in Appendix E.3. We selected two challenging task categories representing different manipulation types prevalent in real-world scenarios:

1. **Open Door:** An articulation task requiring precise interaction with a hinged object. We evaluate on sub-tasks of opening the door to 90° and 180° .

2. **Push T-Block:** A representative long-horizon rearrangement task. We define three sub-tasks: (i) translating the T-block to a target position, (ii) rotating the T-block to a target orientation, and (iii) a combined task of translating and then rotating the T-block.

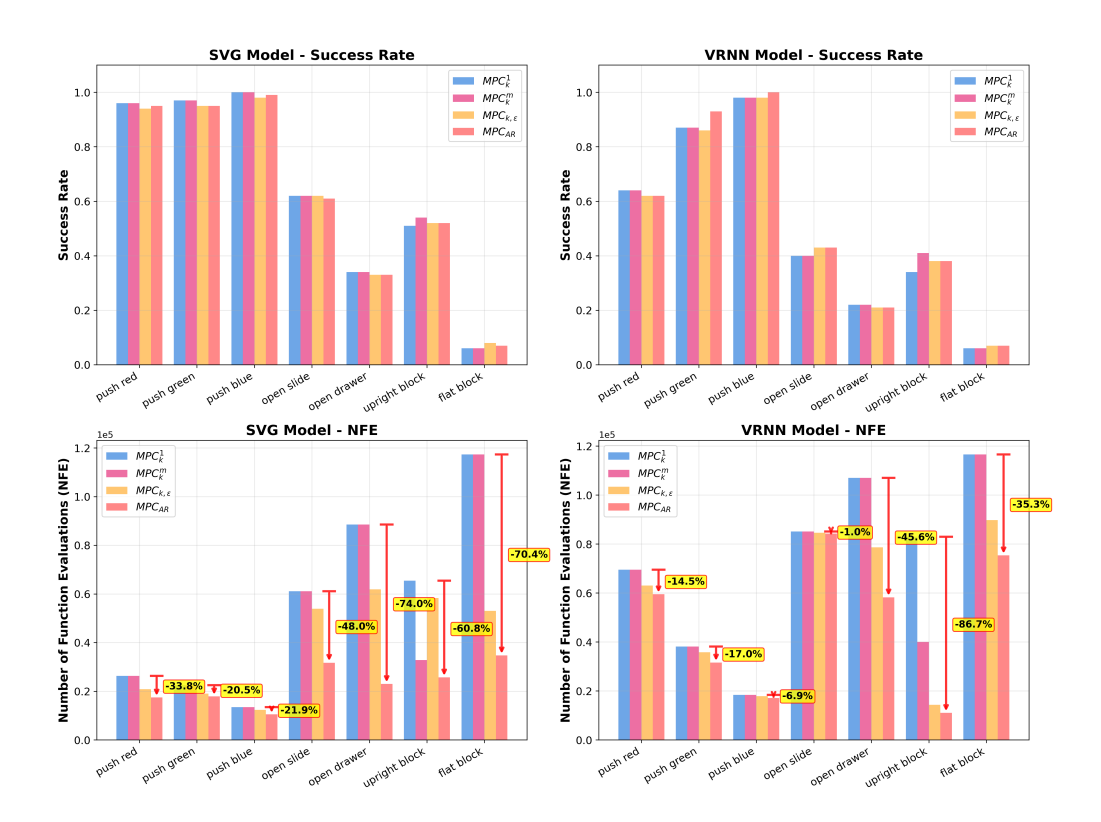


Figure 2: Results in Simulated Experiments. Here we tune the hyperparameter of the algorithms such that the performance are almost the same. It is demonstrated that our adaptive method enjoys most significant computational savings.

4.2 Main Results

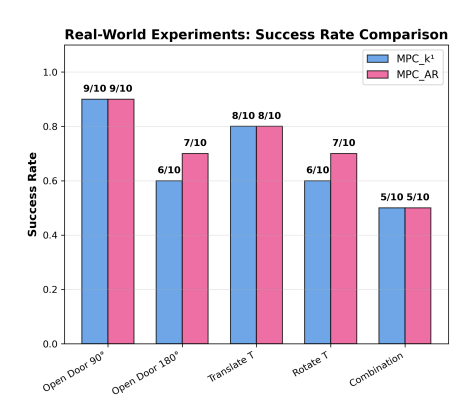
Results in Simulated Experiments For all the algorithms, we tune their hyperparameters such the success rates of all the accelerating methods drop no more than 0.02 compared with standard MPC $_k^1$. From Appendix F.1 we can see that both MPC $_k^m$ and MPC $_{k,\epsilon}$ cannot significantly accelerate computation and guarantee performance simultaneously. MPC $_{AR}$, which adopts adaptive re-planning schedule, have much advantages as shown in Figure 2.

Results in Real-World Experiments Visual demonstrations are detailed in Appendix F.2. Here we only provide quantitative results. As shown in Figure 3, our adaptive approach MPC_{AR} demonstrates significant NFE reduction while maintaining or improving success rates across various sub-tasks. It has much better performance compared with that in the simulator because state-based planning is more explicit than vision-based planning.

4.3 ANAYLSIS AND DISCUSSIONS

ADAREP achieves greater acceleration with accurate predictions. To investigate the impact of prediction accuracy on our adaptive algorithm, we conducted additional experiments using a "disturbed simulator" as the predictive world model which allowed us to directly control the magnitude of prediction errors introduced into the system. Specifically, we added varying levels of Gaussian noise to the true simulated state components (robot position/velocity, object position/velocity, and end-effector position) before feeding them to the planner. We evaluated three distinct levels of disturbance, with further details provided in Appendix E.6 and results are summarized in Figure 7.

ADAREP achieves greater acceleration when system dynamics are smoother. The effective sensitivity of system dynamics can vary considerably, even within a single manipulation task. Consider the "open door" task: the dynamics are often highly sensitive when the end-effector interacts with



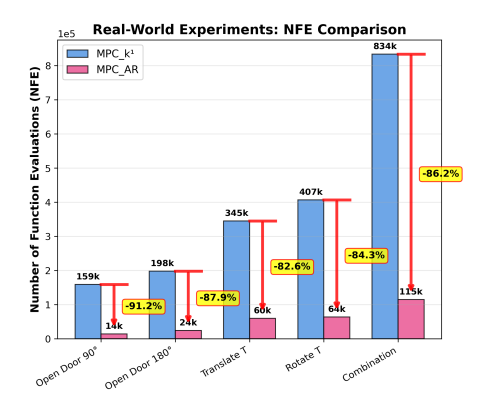


Figure 3: Results in Real-World Experiments. MPC_{AR} can maintain strong performance and enjoy computational savings simultaneously.

the door near its axis of rotation, as small end-effector movements can induce large angular changes. Figure 4 illustrates this concept. ADAREP can reduce re-planning frequency more aggressively, leading to greater computational savings.

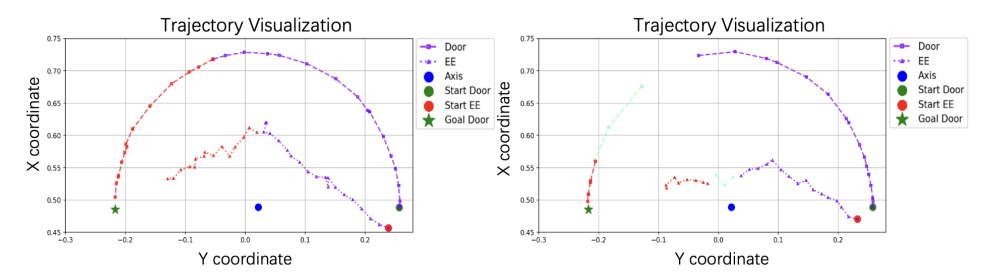


Figure 4: Illustration of varying dynamics sensitivity in the "open door" task. Left: Pushing the door far from its axis often results in more predictable, smoother changes in the door's state per unit of end-effector motion. Right: Pushing very close to the axis can lead to more abrupt or sensitive changes. Different colors represent controls from different plans.

ADAREP maintains performance even in worst-case scenarios. Real-world applications often present challenges such as large, unexpected prediction errors from the world model or highly sensitive, difficult-to-control system dynamics. In such adverse conditions, a key strength of MPC_{AR} is its ability to adapt and prioritize task performance. By continuously monitoring metrics like prediction error (see Figure 5) and estimated local dynamics sensitivity (Figure 6), our algorithm automatically reduces its replanning threshold ϵ_t . This leads to more frequent replanning, effectively causing MPC_{AR} to behave more like standard MPC_k^1 , thereby ensuring robustness and maintaining performance, albeit with reduced computational savings in these demanding situations.

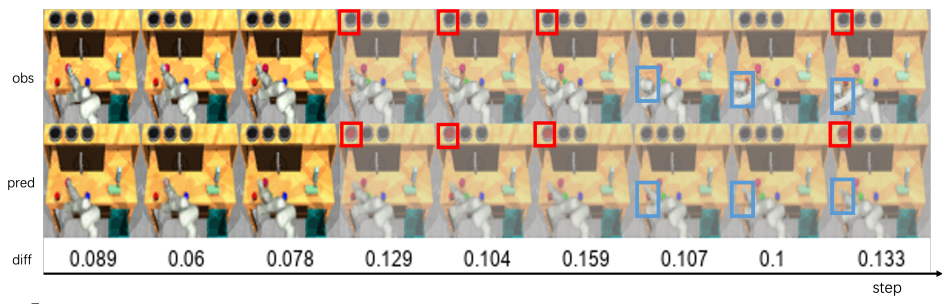


Figure 5: Visualization of prediction error monitoring. The first row shows observed images from the environment. The second row displays the corresponding images predicted by the world model. The third row quantifies the prediction error, likely computed in a feature space as Equation (4) using features from DINO Equation (7). Large discrepancies trigger more frequent replanning.

434

435

436

437

438

439

440

441 442

448

449

450

451

452

453 454 455

456

457

458

459

460

461

462

463

464

465

466

467 468

469

470

471

472

473

474

475 476 477

478 479

480

481

482

483

484

485

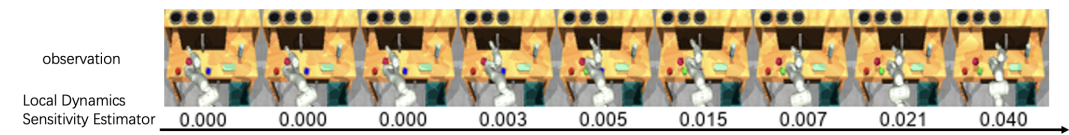


Figure 6: Visualization of local dynamics sensitivity estimation. The top row shows a sequence of observed frames. The bottom row displays the corresponding local dynamics sensitivity estimator \hat{L}_t , computed using Equation (8). Higher values indicate more sensitive dynamics, prompting more frequent replanning.

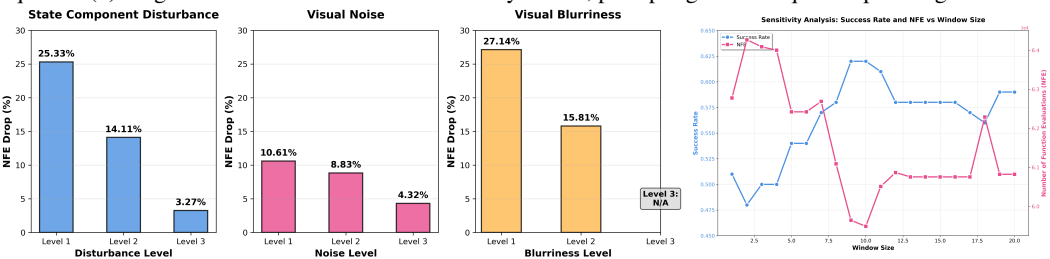


Figure 7: Impact of different levels of state component disturbance, Figure 8: Sensitive Analysis on the visual noise, and visual blurriness on the NFE Drop of ADAREP (relative window size.Small W (e.g., 1-5) reto standard MPC $_k^1$). Success rates were maintained at almost the same sults in poor performance while Large across all tests. Disturbance and corruption parameters are detailed in W (e.g., >15) makes performance Appendix E.6 and Appendix E.7.

plateaus.

ADAREP performs better with more explicit state representations; robust visual features remain a challenge. As observed in Section 4, ADAREP demonstrates significantly better effectiveness when coupled with state-based world models compared to vision-based ones. To investigate the impact of visual input quality on ADAREP when using vision-based world models, we simulated a scenario with a 'perfect' underlying state predictor but introduced various visual corruptions to the image outputs. This was achieved by adding different levels of Gaussian noise or applying Gaussian blur to the images generated by an otherwise accurate simulator (details in Appendix E.7). The results in Figure 7 indicate that even when the underlying state information provided to the planner is perfectly accurate (from the simulator), the performance of ADAREP (when relying on features extracted by DINO from these visually corrupted images) degrades significantly in terms of NFE reduction. This highlights the sensitivity to visual features and suggests that developing more robust visual feature extractors, or methods to better integrate them with adaptive MPC, is a crucial direction for future work.

ADAREP is robust to the choice of window size. We conduct additional experiments on the sensitive analysis of the window size, using the VRNN model. The result in Figure 8 reveals a clear and intuitive trade-off. Small W results in poor performance. We conjecture that the estimates are too unstable and noisy, leading to erratic replanning. Large W makes performance plateaus. The system becomes less responsive, averaging over too much history to react to recent changes. Crucially, the key takeaway is that ADAREP is robust to the choice of W. There is a wide range of values (W from 8 to 16) that yield strong and stable performance.

5 CONCLUSION

This research addressed the computational demands of Model Predictive Control (MPC) with learned world models by introducing ADAREP, an adaptive replanning strategy. Our theoretical analysis elucidated the interplay between replanning frequency, model prediction error, and local dynamics sensitivity, guiding the design of ADAREP which dynamically adjusts its planning effort based on online estimates. This training-free, plug-and-play approach demonstrated significant efficiency gains while preserving or enhancing task success rates. These findings underscore the potential of adaptive replanning for practical robotic control. Future work should focus on developing more robust visual features for vision-based models to broaden its applicability.

6 ETHICS STATEMENT AND REPRODUCIBILITY STATEMENT

Ethics Statement We acknowledge and adhere to the ICLR Code of Ethics. This research focuses on improving computational efficiency in robotic control systems, which has broadly positive societal implications by making robotic automation more accessible and energy-efficient. Our work does not involve human subjects, and all experiments were conducted in controlled simulation environments and with standard robotic hardware. The datasets used (VP2 benchmark, RoboDesk) are publicly available research benchmarks with appropriate licenses. We do not foresee any direct harmful applications of our adaptive replanning methodology, as it is a general computational optimization technique. However, as with any robotics research, we acknowledge that improved robotic capabilities could potentially be misused in harmful applications, though this is far removed from our specific technical contributions. We have no conflicts of interest to declare, and this research was conducted with standard academic integrity practices.

Reproducibility Statement We have made significant efforts to ensure the reproducibility of our work. Our adaptive replanning algorithm (ADAREP) is described in detail in Algorithm 1 with complete implementation details provided in Section 3. All experimental settings are specified in Section 4 and the appendix. The theoretical analysis is complete with full proofs provided in Appendix D. For the simulated experiments, we used the publicly available VP2 benchmark with standard evaluation protocols, and all experimental details are provided in Appendix E. The real-world experimental setup is thoroughly documented in Appendix E.2, including hardware specifications and data collection procedures. We plan to release our implementation code upon acceptance to facilitate reproduction of our results. The baseline methods are implemented using established algorithms from the literature with references provided.

REFERENCES

- Brian DO Anderson and John B Moore. *Optimal control: linear quadratic methods*. Courier Corporation, 2007.
- Andrew Campbell, William Harvey, Christian Weilbach, Valentin De Bortoli, Thomas Rainforth, and Arnaud Doucet. Trans-dimensional generative modeling via jump diffusion models. In A. Oh, T. Naumann, A. Globerson, K. Saenko, M. Hardt, and S. Levine (eds.), *Advances in Neural Information Processing Systems*, volume 36, pp. 42217–42257. Curran Associates, Inc., 2023.
- Mathilde Caron, Hugo Touvron, Ishan Misra, Hervé Jégou, Julien Mairal, Piotr Bojanowski, and Armand Joulin. Emerging properties in self-supervised vision transformers. In *Proceedings of the IEEE/CVF international conference on computer vision*, pp. 9650–9660, 2021.
- Pieter-Tjerk De Boer, Dirk P Kroese, Shie Mannor, and Reuven Y Rubinstein. A tutorial on the cross-entropy method. *Annals of operations research*, 134:19–67, 2005.
- Jingtao Ding, Yunke Zhang, Yu Shang, Yuheng Zhang, Zefang Zong, Jie Feng, Yuan Yuan, Hongyuan Su, Nian Li, Nicholas Sukiennik, Fengli Xu, and Yong Li. Understanding world or predicting future? a comprehensive survey of world models, November 2024.
- Ilgin Dogan, Zuo-Jun Max Shen, and Anil Aswani. Regret analysis of learning-based mpc with partially-unknown cost function, January 2023.
- Yilun Du, Sherry Yang, Bo Dai, Hanjun Dai, Ofir Nachum, Josh Tenenbaum, Dale Schuurmans, and Pieter Abbeel. Learning universal policies via text-guided video generation. *Advances in neural information processing systems*, 36:9156–9172, 2023.
- Anthony V Fiacco and Yo Ishizuka. Sensitivity and stability analysis for nonlinear programming. *Annals of Operations Research*, 27(1):215–235, 1990.
- Manan Gandhi, Bogdan Vlahov, Jason Gibson, Grady Williams, and Evangelos A. Theodorou. Robust model predictive path integral control: Analysis and performance guarantees. *IEEE Robotics and Automation Letters*, 6(2):1423–1430, April 2021. ISSN 2377-3766, 2377-3774. doi: 10.1109/LRA.2021.3057563.

- Gautam Goel, Yiheng Lin, Haoyuan Sun, and Adam Wierman. Beyond online balanced descent: An optimal algorithm for smoothed online optimization. *Advances in Neural Information Processing Systems*, 32, 2019.
 - Jonathan Ho, Ajay Jain, and Pieter Abbeel. Denoising diffusion probabilistic models. *Advances in neural information processing systems*, 33:6840–6851, 2020.
 - Harini Kannan, Danijar Hafner, Chelsea Finn, and Dumitru Erhan. Robodesk: A multi-task reinforcement learning benchmark, 2021.
 - Yingying Li, Guannan Qu, and Na Li. Online optimization with predictions and switching costs: Fast algorithms and the fundamental limit. *IEEE Transactions on Automatic Control*, 66(10): 4761–4768, 2020.
 - Yiheng Lin, Yang Hu, Guanya Shi, Haoyuan Sun, Guannan Qu, and Adam Wierman. Perturbation-based regret analysis of predictive control in linear time varying systems. *Advances in Neural Information Processing Systems*, 34:5174–5185, 2021.
 - Yiheng Lin, Yang Hu, Guannan Qu, Tongxin Li, and Adam Wierman. Bounded-regret mpc via perturbation analysis: Prediction error, constraints, and nonlinearity. *Advances in Neural Information Processing Systems*, 35:36174–36187, 2022.
 - Matthias Minderer, Chen Sun, Ruben Villegas, Forrester Cole, Kevin P Murphy, and Honglak Lee. Unsupervised learning of object structure and dynamics from videos. *Advances in Neural Information Processing Systems*, 32, 2019.
 - Sen Na and Mihai Anitescu. Superconvergence of online optimization for model predictive control. *IEEE Transactions on Automatic Control*, 68(3):1383–1398, 2022.
 - Aaditya Prasad, Kevin Lin, Jimmy Wu, Linqi Zhou, and Jeannette Bohg. Consistency policy: Accelerated visuomotor policies via consistency distillation. *arXiv preprint arXiv:2405.07503*, 2024.
 - Robin Rombach, Andreas Blattmann, Dominik Lorenz, Patrick Esser, and Björn Ommer. High-resolution image synthesis with latent diffusion models. In *Proceedings of the IEEE/CVF conference on computer vision and pattern recognition*, pp. 10684–10695, 2022.
 - Sungho Shin and Victor M Zavala. Controllability and observability imply exponential decay of sensitivity in dynamic optimization. *IFAC-PapersOnLine*, 54(6):179–184, 2021.
 - Sungho Shin, Victor M Zavala, and Mihai Anitescu. Decentralized schemes with overlap for solving graph-structured optimization problems. *IEEE Transactions on Control of Network Systems*, 7(3): 1225–1236, 2020.
 - Haotian Sun, Yuchen Zhuang, Lingkai Kong, Bo Dai, and Chao Zhang. Adaplanner: Adaptive planning from feedback with language models. *Advances in neural information processing systems*, 36:58202–58245, 2023.
 - Stefan CM ten Eikelder and Jacobus HM van Amerongen. Resource allocation problems with expensive function evaluations. *European Journal of Operational Research*, 306(3):1170–1185, 2023.
 - Stephen Tian, Yancheng Cai, Hong-Xing Yu, Sergey Zakharov, Katherine Liu, Adrien Gaidon, Yunzhu Li, and Jiajun Wu. Multi-object manipulation via object-centric neural scattering functions. In *Proceedings of the IEEE/CVF Conference on Computer Vision and Pattern Recognition (CVPR)*, pp. 9021–9031, June 2023a.
 - Stephen Tian, Chelsea Finn, and Jiajun Wu. A control-centric benchmark for video prediction. In *International Conference on Learning Representations*, 2023b.
 - Ruben Villegas, Arkanath Pathak, Harini Kannan, Dumitru Erhan, Quoc V Le, and Honglak Lee. High fidelity video prediction with large stochastic recurrent neural networks. *Advances in Neural Information Processing Systems*, 32, 2019.

Xiaofeng Wang, Zheng Zhu, Guan Huang, Xinze Chen, Jiagang Zhu, and Jiwen Lu. Drivedreamer: Towards real-world-drive world models for autonomous driving. In *European Conference on Computer Vision*, pp. 55–72. Springer, 2024.

Grady Williams, Nolan Wagener, Brian Goldfain, Paul Drews, James M. Rehg, Byron Boots, and Evangelos A. Theodorou. Information theoretic MPC for model-based reinforcement learning. In 2017 IEEE International Conference on Robotics and Automation (ICRA), pp. 1714–1721, May 2017. doi: 10.1109/ICRA.2017.7989202.

Jialong Wu, Shaofeng Yin, Ningya Feng, Xu He, Dong Li, Jianye Hao, and Mingsheng Long. ivideogpt: Interactive videogpts are scalable world models. *Advances in Neural Information Processing Systems*, 37:68082–68119, 2024.

Wanting Xu and Mihai Anitescu. Exponentially convergent receding horizon strategy for constrained optimal control. *Vietnam Journal of Mathematics*, 47(4):897–929, 2019.

Mengjiao Yang, Yilun Du, Kamyar Ghasemipour, Jonathan Tompson, Dale Schuurmans, and Pieter Abbeel. Learning interactive real-world simulators. *arXiv preprint arXiv:2310.06114*, 1(2):6, 2023.

Wentao Zhao, Jiaming Chen, Ziyu Meng, Donghui Mao, Ran Song, and Wei Zhang. Vlmpc: Vision-language model predictive control for robotic manipulation. In *Robotics: Science and Systems*, 2024.

A THE USE OF LARGE LANGUAGE MODELS (LLMS)

We acknowledge the use of Large Language Models (LLMs) in this work for the following specific tasks:

- Writing assistance: Grammar checking, sentence restructuring, and improving clarity of exposition.
- Code implementation: Implementing well-established baseline methods (CEM, MPPI) based on existing literature.
- **Visualization:** Generating and refining figures for data presentation.

Importantly, all core contributions of this work were conceived and developed entirely by the authors: the adaptive replanning idea, theoretical analysis and proofs, experimental design, novel algorithmic contributions, interpretation of results, and all scientific insights and conclusions. LLMs were not used for any creative, analytical, or decision-making aspects of the research.

B ALGORITHM PSEUDOCODES

Algorithm 2 Model Predictive Control (MPC $_{k}^{1}$)

Require: Prediction horizon k, initial state x(0), access to predictions $\xi_{\tau:\tau'|\tau}$, terminal cost function F_T . (Specify intermediate terminal costs F_t for $k \le t < T$ if needed for stability/performance).

- 1: **for** $t = 0, 1, \dots, T 1$ **do**
- 2: $t' \leftarrow \min\{t + k, T\}$
- 3: Observe current state x_t and obtain predictions $\xi_{t:t'|t}$.
- 4: Define terminal cost for subproblem: $F_{term} = F_{t'}$ if t' < T else F_T .
- 5: Define terminal parameter for subproblem: $\zeta_{term} = \xi_{t'|t}$.
- 6: Solve for $(y_{t:t'}, v_{t:t'-1}) = \psi_t^{t'}(x_t, \xi_{t:t'-1|t}, \zeta_{term}; F_{term}).$
- 7: Commit the first control action: $u_t := v_t$.

C THEORETICAL ANALYSIS

This section provides the detailed theoretical analysis underpinning our results, including assumptions, key technical lemmas, and regret bounds.

654

655

656

657

658

659

660

661

662

663

665

678

679

680

681

682

683

684

685

686

687

688 689

690

691

692

693

694

696

697

700 701 1: $t \leftarrow 0$

Algorithm 3 Model Predictive Control with Fixed Replan Frequency (MPC $_k^m$)

Require: Prediction horizon k, replan frequency m $(1 \le m \le k)$, initial state x(0), access to predictions $\xi_{\tau:\tau'|\tau}$, terminal cost function F_T . (Specify intermediate terminal costs F_t for $k \le t < T$ if needed).

```
2: while t < T do
3:
         t' \leftarrow \min\{t + k, T\}
4:
         Observe current state x_t and obtain predictions \xi_{t:t'|t}.
         Define terminal cost for subproblem: F_{term} = F_{t'} if t' < T else F_T.
5:
         Define terminal parameter for subproblem: \zeta_{term} = \xi_{t'|t}.
6:
         Solve for (y_{t:t'}, v_{t:t'-1}) = \psi_t^{t'}(x_t, \xi_{t:t'-1|t}, \zeta_{term}; F_{term}).
7:
         Determine number of steps to commit: m_{commit} = \min(m, T - t).
8:
9:
         Commit the first m_{commit} control actions: u_{\tau} := v_{\tau} for \tau = t, \dots, t + m_{commit} - 1.
10:
         t \leftarrow t + m_{commit}
```

Algorithm 4 Model Predictive Control with Fixed Threshhold (MPC $_{k,\epsilon}$)

Require: Prediction horizon k, threshold ϵ , initial state x(0), access to predictions $\xi_{\tau:\tau'\mid\tau}$, terminal cost function F_T . (Specify intermediate terminal costs F_t for $k \leq t < T$ if needed).

```
1: t \leftarrow 0
 2: t_{plan} \leftarrow 0
 3: while t < T do
 4:
          if t == t_{plan} then
               t' \leftarrow \min\{t+k,T\}
 5:
               Observe current state x_t and obtain predictions \xi_{t:t'|t}.
 6:
 7:
              Define terminal cost F_{term} = F_{t'} if t' < T else F_T.
 8:
               Define terminal parameter \zeta_{term} = \xi_{t'|t}.
               Solve for: (y_{t:t'}, v_{t:t'-1}) = \psi_t^{t'}(x_t, \xi_{t:t'-1|t}, \zeta_{term}; F_{term}).
 9:
10:
          u_t := v_t.
11:
          Execute action u_t in environment.
          Observe next state x_{t+1}.
12:
          if ||x_{t+1} - y_{t+1}|| > \epsilon then
13:
14:
               t_{plan} \leftarrow t + 1
          else
15:
              if t+1 == t' then
16:
17:
                   t_{plan} \leftarrow t + 1
18:
          t \leftarrow t + 1
```

708

709 710

742

743

744

745

746

747 748

749

Algorithm 5 Model Predictive Control with Adaptive Re-Planning (ADAREP) (MPC_{AR})

Require: Prediction horizon k, threshold ϵ , initial state x(0), access to predictions $\xi_{\tau:\tau'\mid\tau}$, terminal cost function F_T . (Specify intermediate terminal costs F_t for $k \leq t < T$ if needed).

```
1: t \leftarrow 0
711
            2: t_{plan} \leftarrow 0
712
            3: while t < T do
713
                    if t == t_{plan} then
714
            5:
                         t' \leftarrow \min\{t+k,T\}
715
            6:
                         Observe current state x_t and obtain predictions \xi_{t:t'|t}.
716
                         Define terminal cost F_{term} = F_{t'} if t' < T else F_T.
            7:
717
                         Define terminal parameter \zeta_{term} = \xi_{t'|t}.
            8:
718
                         Solve for: (y_{t:t'}, v_{t:t'-1}) = \psi_t^{t'}(x_t, \xi_{t:t'-1|t}, \zeta_{term}; F_{term}).
            9:
719
           10:
                    u_t := v_t.
720
                    Execute action u_t in environment.
           11:
721
           12:
                    Observe next state x_{t+1}.
722
           13:
                    Update threshold \epsilon_{t+1} using Algorithm 1
723
           14:
                    if ||x_{t+1} - y_{t+1}|| > \epsilon_{t+1} then
724
                         t_{plan} \leftarrow t + 1
           15:
725
           16:
                    else
726
                         if t+1 == t' then
           17:
727
                              t_{plan} \leftarrow t + 1
           18:
728
           19:
                    t \leftarrow t + 1
729
```

Algorithm 6 ADAREP: Adaptive Re-Planning Threshold Update (practical version)

Require: Buffers \mathcal{D}_{δ} , \mathcal{D}_{L} , action u_{t} , prediction y_{t+1} , base threshold ϵ_{t}

- 1: Calculate prediction error δ^o_t using Eq. equation 4
- 2: Estimate local dynamics sensitivity L_t by

$$\widehat{L}_{t} = \frac{\|x_{t+1} - x_{t}\|}{\|u_{t}\| + \varepsilon} \,, \tag{8}$$

- 3: Update buffer $\mathcal{D}_{\delta} \leftarrow \text{UPDATEBUF}(\mathcal{D}_{\delta}, \delta, W), \mathcal{D}_{L} \leftarrow \text{UPDATEBUF}(\mathcal{D}_{L}, \widehat{L}, W)$
- 4: Update the threshold $\epsilon_t \leftarrow \epsilon_0 \cdot \exp(-\alpha_\delta \operatorname{mean}(\mathcal{D}_\delta)) \cdot \exp(-\alpha_L \operatorname{mean}(\mathcal{D}_L))$

Table 2: Summary of theoretical regret bounds and NFE. Here, $L = \max_{0 \le t < T} L_t$ and $L_* = \max_{0 \le t \le T} \max_{0 \le i \le m-1} \prod_{s=t}^{t+i} L_s$ characterize the sensitivity (Lipschitz constants) of the dynamics over single and multiple steps, respectively. E represent cumulative prediction errors of the underlying model; they have slightly different forms but are conceptually similar for comparison purposes. Note that when m=1 or $\epsilon=0$, our results recover (Lin et al., 2022). And S is the sample size of the planner at each step. $N_{\epsilon}, N_{\epsilon, \alpha} \le T$ is the total number of plans that decreases as ϵ, α_L and α_δ increases.

| Algorithm | Regret Bound | NFE |
|--------------------|---|------------------------|
| MPC^1_k | $O\left(\sqrt{L^2 \mathrm{cost}(OPT) \cdot E} + L^2 E\right)$ | TkS |
| MPC^m_k | $O\left(\sqrt{mL_*^2\mathrm{cost}(OPT)\cdot E} + mL_*^2E ight)$ | $\lceil T/m \rceil kS$ |
| $MPC_{k,\epsilon}$ | $O\left(\sqrt{L^2 \mathrm{cost}(OPT) \cdot (E + \epsilon E + \epsilon^2 T)} + L^2(E + \epsilon E + \epsilon^2 T)\right)$ | $N_{\epsilon}kS$ |
| MPC_{AR} | $O\left(\sqrt{\cos(OPT)(L^2E + \frac{\epsilon_0}{\alpha_L^2}(\epsilon_0 + \frac{1}{\alpha_\delta})T}) + L^2E + \frac{\epsilon_0}{\alpha_L^2}(\epsilon_0 + \frac{1}{\alpha_\delta})T\right)$ | $N_{\epsilon,lpha}kS$ |

C.1 ASSUMPTIONS AND NOTATIONS

Our analysis largely follows the framework established by Lin et al. (2022). We impose the following standard assumptions throughout this section:

- Stability of OPT: The offline optimal trajectory $(x_{0:T}^*, u_{0:T-1}^*)$ is bounded. There exists a constant $D_{x^*} > 0$ such that $||x_t^*|| \le D_{x^*}$ for all states x_t^* on the optimal trajectory $(0 \le t \le T)$.
- Lipschitz Dynamics: The ground-truth dynamics function $g_t(\cdot, \cdot; \xi_t^*)$ is Lipschitz continuous with respect to both state and action. There exists a constant L_t such that for any feasible states x_t, x_t' and actions u_t, u_t' :

$$||g_t(x_t, u_t; \xi_t^*) - g_t(x_t', u_t'; \xi_t^*)|| \le L_t(||x_t - x_t'|| + ||u_t - u_t'||).$$
(9)

• Cost Function Regularity: Every stage cost $f_t(\cdot,\cdot;\xi_t^*)$ and the terminal cost $F_T(\cdot;\xi_T^*)$ are non-negative, convex, and ℓ -smooth with respect to (x_t,u_t) and x_T , respectively, for some $\ell > 0$.

We note a slight strengthening compared to Lin et al. (2022), who only required the dynamics $g_t(\cdot,\cdot;\xi_t^*)$ to be Lipschitz continuous with respect to the action u_t . Our stronger assumption (Lipschitz continuity w.r.t. both state x_t and action u_t) is utilized specifically in the analysis of MPC_k^m (Algorithm 3). The analysis for $\mathsf{MPC}_{k,\epsilon}$ (Algorithm 4) does not require this modification and holds under the weaker assumption.

When the context is clear, we use the shorthand $g_t(\cdot,\cdot) := g_t(\cdot,\cdot;\xi_t^*)$, $f_t(\cdot,\cdot) := f_t(\cdot,\cdot;\xi_t^*)$, and $F_T(\cdot) := F_T(\cdot;\xi_T^*)$ to simplify notation.

C.2 PERTURBATION ANALYSIS

Our analysis relies heavily on perturbation bounds for the Finite-Time Optimal Control Problem (FTOCP, see Definition 2.1), which characterize how the optimal solution changes in response to perturbations in parameters or initial states. Prior works (Shin et al., 2020; Lin et al., 2021; Shin & Zavala, 2021; Xu & Anitescu, 2019; Na & Anitescu, 2022) have established such bounds, often locally, for various FTOCP instances. We adopt the generalized forms presented by Lin et al. (2022):

(a) Parameter Perturbations (fixed initial state z): Let $\psi_{t_1}^{t_2}(z,\xi;F)_v$ denote the optimal control sequence from the FTOCP solution. Then,

$$\left\| \psi_{t_1}^{t_2} \left(z, \xi_{t_1:t_2}; F \right)_{v_t} - \psi_{t_1}^{t_2} \left(z, \xi_{t_1:t_2}'; F \right)_{v_t} \right\| \le \left(\sum_{s=t_1}^{t_2} q_1(s-t_1) \delta_s \right) \|z\| + \sum_{s=t_1}^{t_2} q_2(s-t_1) \delta_s,$$
(10)

where $\delta_s := \|\xi_s - \xi_s'\|$ for $s \in [t_1, t_2]$. The scalar functions q_1, q_2 represent sensitivity decay and satisfy $\lim_{t \to \infty} q_i(t) = 0$ and $\sum_{t=0}^{\infty} q_i(t) \le C_i$ for constants $C_i \ge 1$, i = 1, 2.

(b) Initial State Perturbation (fixed parameters ξ): Let $\psi_{t_1}^{t_2}(z,\xi;F)_{y_t/v_t}$ denote the state or control component at time t of the optimal solution. Then,

$$\left\| \psi_{t_1}^{t_2} \left(z, \xi_{t_1:t_2}; F \right)_{y_t/v_t} - \psi_{t_1}^{t_2} \left(z', \xi_{t_1:t_2}; F \right)_{y_t/v_t} \right\| \le q_3(t-t_1) \left\| z - z' \right\|, \text{ for } t \in [t_1, t_2],$$
 (11)

where the sensitivity decay function q_3 satisfies $\sum_{t=0}^{\infty} q_3(t) \leq C_3$ for some constant $C_3 \geq 1$.

Intuitively, bound equation 10 suggests that errors in parameter predictions further in the future have a diminishing impact on the current optimal action. Bound equation 11 implies a form of stability: the effect of an initial state perturbation decays over time within the planned trajectory.

While these perturbation bounds are powerful, proving they hold globally can be challenging; often, they are established locally around a nominal trajectory. For a practical predictive control system designed to track an optimal trajectory, it is reasonable to expect the executed trajectory to remain relatively close to the (unknown) optimal one. Building on this, we adopt the following property, similar to Lin et al. (2022), which posits that these bounds hold within a certain region around the optimal trajectory OPT. Let $\mathcal{B}(x,R)$ denote the closed ball of radius R centered at x.

Property C.1. There exists a constant $R_1 > 0$ such that the perturbation bounds equation 10 and equation 11 hold under the following specifications, assuming the underlying parameter sets Ξ_t contain the relevant parameters:

- Bound equation 10 holds for $t_1 = t, t_2 = t + k$ (where t < T k) with terminal function $F = \mathbb{I}$ (identity), initial state $z \in \mathcal{B}(x_t^*, R_1)$, parameters $\xi'_{t:t+k-1} = \xi^*_{t:t+k-1}$ (ground truth), and $\xi_{t:t+k}$ being any valid parameters within the family.
- Bound equation 10 holds for $t_1 = t, t_2 = T$ (where $t \ge T k$) with terminal function $F = F_T$, initial state $z \in \mathcal{B}(x_t^*, R_1)$, parameters $\xi'_{t:T} = \xi^*_{t:T}$, and $\xi_{t:T}$ being any valid parameters.
- Bound equation 11 holds for any t_1, t_2 , any initial states $z, z' \in \mathcal{B}(x_{t_1}^*, R_1)$, and ground-truth parameters $\xi_{t_1:t_2} = \xi_{t_1:t_2}^*$.

We quantify the quality of the parameter predictions $\xi_{t+\tau|t}$ (prediction of $\xi_{t+\tau}^*$ made at time t) available to the online controller.

Definition C.1 (Prediction Error). The prediction error at time t for lead time $\tau \geq 0$ is $\rho_{t,\tau} \coloneqq \|\xi_{t+\tau}\|_{t} - \xi_{t+\tau}^*\|_{t}$.

A key challenge in analyzing online algorithms via regret is the state mismatch: the online algorithm's state x_t generally differs from the offline optimal state x_t^* . Directly comparing the online action u_t to the offline optimal action u_t^* is therefore insufficient. Inspired by techniques in reinforcement learning (Lin et al., 2021), Lin et al. (2022) utilized a per-step error comparing the online action u_t to the optimal action $u_{t|t}^*$ from the *current* state x_t . For analyzing MPC_k^m , where actions are based on plans made at earlier times t', we introduce a conditional variant.

Definition C.2 (Per-Step Error). The per-step error e_t incurred by a predictive online controller ALG at time step t is defined as the distance between its actual action u_t and the clairvoyant optimal action, i.e.,

$$e_t := \|u_t - u_{t|t}^*\| = \|u_t - \psi_t^T(x_t, \xi_{t:T}^*; F_T)_{v_t}\|, \text{ where } u_t = \mathsf{ALG}(x_t, \xi_{t:t+k|t})_{v_t}.$$

The clairvoyant optimal trajectory starting from x_t is defined as $x_{t:T|t}^* := \psi_t^T(x_t, \xi_{t:T}^*; F_T)_{y_{t:T}}$.

Definition C.3 (Conditional Per-Step Error). The conditional per-step error e_t incurred by a predictive online controller ALG at time step t given time step t' is defined as the distance between its actual action u_t and the clairvoyant optimal action given t'

$$e_{t|t'} \coloneqq \left\| u_t - u_{t|t'}^* \right\| = \left\| u_t - \psi_{t'}^T(x_{t'}, \xi_{t':T}^*; F_T)_{v_t} \right\|, \text{ where } u_t = \mathsf{ALG}(x_{t'}, \xi_{t':t'+k|t'})_{v_t}.$$

The clairvoyant optimal trajectory starting from x_t is defined as $x_{t:T|t}^* := \psi_t^T(x_t, \xi_{t:T}^*; F_T)_{y_{t:T}}$.

What's described above are adequate to analyze the regret of MPC_k^m (Algorithm 3) and $MPC_{k,\epsilon}$ (Algorithm 4). However, when it comes to the analysis of MPC_{AR} (Algorithm 5), additional assumptions have to be made.

The core idea of ADAREP is to monitor and estimate local dynamic sensitivity and prediction error based on observation. Previous assumptions only characterize how performance or deviation can be upper bounder by local dynamic sensitivity and prediction error, but do not reveal how local dynamic sensitivity and prediction error can be estimated by ground-truth observation. In the light of this, we introduce the following properties, which gives the inequalities on the opposite direction of eq. (9) and Equation (10).

• Lipschitz Dynamics: For all $||u_t|| > 0$, there exist $0 < \lambda < 0$ such that

$$\lambda L_t \|u_t\| \le \|g_t(x_t, u_t; \xi_t^*) - x_t\| \le L_t \|u_t\|$$
.

• Parameter Perturbations: There exist $0 < \mu < 0$ such that

$$\left\| \psi_{t_1}^{t_2}(z, \xi_{t_1:t_2}; F)_{y_t} - \psi_{t_1}^{t_2}(z, \xi'_{t_1:t_2}; F)_{y_t} \right\| \ge \mu \left(\sum_{s=t_1}^{t_2} q_1(s-t_1) \delta_s \right) \|z\| + \mu \sum_{s=t_1}^{t_2} q_2(s-t_1) \delta_s,$$
(12)

Now we are ready to provide the regret analysis for all the algorithms.

C.3 REGRET ANALYSIS FOR MPC_k^m

We first bound the conditional per-step error for the MPC_k^m algorithm.

Lemma C.1 (Conditional Per-Step Error Bound). Assume Property C.1 holds. Let $t' = mn \le t < m(n+1)$. Assume the state at the last replanning time satisfies $x_{t'} \in \mathcal{B}(x_{t'}^*, R_1)$. Further assume the (potentially hypothetical) terminal cost used within the FTOCP solved at time t' implies a target terminal state $\bar{y}(\xi_{t'+k|t'}) \in \mathcal{B}(x_{t'+k}^*, R_2)$ for some constant $R_2 \ge R_1 > 0$. Then, the conditional per-step error $e_{t|t'}$ of MPC_k^m is bounded by:

$$e_{t|t'} \le \sum_{\tau=0}^{k} \left(\left(R_1 + D_{x^*} \right) \cdot q_1(\tau) + q_2(\tau) \right) \rho_{t',\tau} + 2R_2 \left(\left(R_1 + D_{x^*} \right) \cdot q_1(k) + q_2(k) \right) . \tag{13}$$

Next, we relate the deviation from the clairvoyant optimal trajectory (starting from $x_{t'}$) to these conditional errors.

Lemma C.2 (State Deviation Bound). Let $t' = mn \le t < m(n+1)$ and let $x_{\tau|t'}^*$ denote the state at time τ on the clairvoyant optimal trajectory starting from $x_{t'}$ at time t'. Under the Lipschitz dynamics assumption, we have:

$$\left\| x_t - x_{t|t'}^* \right\| \le \sum_{\tau = t'}^{t-1} e_{\tau|t'} \left(\prod_{s = \tau + 1}^{t-1} L_s \right) .$$
 (14)

The following lemma connects the cumulative conditional per-step errors to the dynamic regret, analogous to Lemma 3.2 in Lin et al. (2022).

Lemma C.3 (Regret Bound via Conditional Errors). Assume T = mN for integer N. Let $L_* = \max_{0 \le t \le T-k} \prod_{s=t}^{t+k-1} L_s$. Under the assumptions on cost function regularity and the applicability of perturbation bound equation 11 (Property C.1), the dynamic regret of MPC_k^m is upper bounded by:

$$cost(\mathsf{MPC}_{k}^{m}) - cost(\mathsf{OPT})$$

$$\leq \sqrt{\left(\frac{\ell}{2} \cdot 2mL_{*}^{2}C_{3}^{2}\right) \cdot cost(\mathsf{OPT}) \cdot \left(\sum_{i=0}^{N-1} \sum_{\tau=mi}^{m(i+1)-1} e_{\tau|mi}^{2}\right)}$$

$$+ \frac{\ell}{2} \cdot 2mL_{*}^{2}C_{3}^{2} \left(\sum_{i=0}^{N-1} \sum_{\tau=mi}^{m(i+1)-1} e_{\tau|mi}^{2}\right) . \tag{15}$$

Combining these results yields the main regret theorem for MPC_k^m .

Theorem C.4 (Regret Bound for MPC_k^m). Let Property C.1 hold. Suppose the terminal cost F_{t+k} of MPC_k^m is set to be the indicator function of some state $\bar{y}(\xi_{t+k|t})$ that satisfies $\bar{y}(\xi_{t+k|t}) \in \mathcal{B}(x_{t+k}^*, R_2)$ for all time steps t < T - k. Further, suppose the prediction errors $\rho_{t,\tau}$ are sufficiently small and the prediction horizon k is sufficiently large, such that

$$\sum_{\tau=0}^{k} \left(\left(R_1 + D_{x^*} \right) \cdot q_1(\tau) + q_2(\tau) \right) \rho_{mn,\tau} + 2R_2 \left(\left(R_1 + D_{x^*} \right) \cdot q_1(k) + q_2(k) \right) \le \frac{R_1}{mC_3L_*} .$$

Then, the trajectory of MPC_k^m will remain close to OPT, i.e. $x_t \in \mathcal{B}(x_t^*, R_1)$ for all time steps t, and the dynamic regret of MPC_k^m is upper bounded by

$$cost(\mathsf{MPC}_k^m) - cost(\mathsf{OPT}) = O\left(\sqrt{mL_*^2 cost(\mathsf{OPT}) \cdot E_1} + mL_*^2 E_1\right),\tag{16}$$

where
$$E_1 = O\left(\sum_{\tau=0}^{k-1} \left(R_0 \cdot q_1(\tau) + q_2(\tau)\right) \sum_{n=0}^{N} m \rho_{mn,\tau}^2 + \left(q_1(k)^2 + q_2(k)^2\right) T\right)$$
.

C.4 REGRET ANALYSIS FOR $MPC_{k,\epsilon}$.

We first bound the per-step error of $MPC_{k,\epsilon}$.

Lemma C.5. Let Property C.1 hold. Suppose the current state x_t satisfies $x_t \in \mathcal{B}(x_t^*, R_1)$ and the terminal cost F_{t+k} of $\mathsf{MPC}_{k,\epsilon}$ is set to be the indicator function of some state $\bar{y}(\xi_{t+k|t})$ that satisfies $\bar{y}(\xi_{t+k|t}) \in \mathcal{B}(x_{t+k}^*, R_2)$ for t < T - k. Further, suppose the last planned time step is t'. Then, the per-step error of $\mathsf{MPC}_{k,\epsilon}$ and MPC_{AR} is bounded by

$$e_t \le q_3(0)\epsilon + \sum_{\tau=0}^k \left((R_1 + D_{x^*}) \cdot q_1(\tau) + q_2(\tau) \right) \rho_{t',\tau} + 2R_2 \left((R_1 + D_{x^*}) \cdot q_1(k) + q_2(k) \right) . \tag{17}$$

This yields the final regret bonud for $MPC_{k,\epsilon}$.

Theorem C.6 (Regret Bound for $\mathsf{MPC}_{k,\epsilon}$). Let Property C.1 hold. Suppose the terminal cost F_{t+k} of MPC_k^m is set to be the indicator function of some state $\bar{y}(\xi_{t+k|t})$ that satisfies $\bar{y}(\xi_{t+k|t}) \in \mathcal{B}(x_{t+k}^*, R_1)$ for all time steps t < T - k. Let $L = \max_{0 \le t \le T} L_t$ Further, suppose the prediction errors $\rho_{t,\tau}$ and threshold ϵ are sufficiently small and the prediction horizon k is sufficiently large, such that

$$q_3(0)\epsilon + \sum_{\tau=0}^k \left(\left(R_1 + D_{x^*} \right) \cdot q_1(\tau) + q_2(\tau) \right) \rho_{t,\tau} + 2R_2 \left(\left(R_1 + D_{x^*} \right) \cdot q_1(k) + q_2(k) \right) \le \frac{R_1}{C_3 L} .$$

Then, the trajectory of $MPC_{k,\epsilon}$ will remain close to OPT, i.e. $x_t \in \mathcal{B}(x_t^*, R_1)$ for all time steps t, and the dynamic regret of $MPC_{k,\epsilon}$ is upper bounded by

$$cost(\mathsf{MPC}_{k,\epsilon}) - cost(\mathsf{OPT}) = O\left(\sqrt{L^2 cost(\mathsf{OPT}) \cdot (E_2 + \epsilon E_2 + \epsilon^2 T)} + mL_*^2(E_2 + \epsilon E_2 + \epsilon^2 T)\right),\tag{18}$$

where $E_2 = O\left(\sum_{\tau=0}^{k-1} (R_0 \cdot q_1(\tau) + q_2(\tau)) \sum_{t=0}^{T} \rho_{p(t),\tau}^2 + (q_1(k)^2 + q_2(k)^2) T\right)$, p(t) denotes the last time step that plans before t.

C.5 REGRET ANALYSIS FOR MPC_{AR} .

Theorem C.7 (Regret Bound for MPC_{AR}). Let Property C.1 hold. Suppose the terminal cost F_{t+k} of MPC $_k^m$ is set to be the indicator function of some state $\bar{y}(\xi_{t+k|t})$ that satisfies $\bar{y}(\xi_{t+k|t}) \in \mathcal{B}(x_{t+k}^*, R_1)$ for all time steps t < T - k. Let $L = \max_{0 \le t \le T} L_t$ Further, suppose the prediction errors $\rho_{t,\tau}$ and threshold ϵ are sufficiently small and the prediction horizon k is sufficiently large, such that

$$q_3(0)\epsilon + \sum_{\tau=0}^k \left(\left(R_1 + D_{x^*} \right) \cdot q_1(\tau) + q_2(\tau) \right) \rho_{t,\tau} + 2R_2 \left(\left(R_1 + D_{x^*} \right) \cdot q_1(k) + q_2(k) \right) \le \frac{R_1}{C_3 L} .$$

Then, the trajectory of $\mathsf{MPC}_{k,\epsilon}$ will remain close to OPT , i.e. $x_t \in \mathcal{B}(x_t^*, R_1)$ for all time steps t, and the dynamic regret of $\mathsf{MPC}_{k,\epsilon}$ is upper bounded by

$$cost(\mathsf{MPC}_{k,\epsilon}) - cost(\mathsf{OPT})$$

$$= O\left(\min\left\{Regret(\mathsf{MPC}_{k,\epsilon_0}), \sqrt{cost(\mathsf{OPT})(L^2E + \frac{\epsilon_0}{\alpha_L^2}(\epsilon_0 + \frac{1}{\alpha_\delta})T) + L^2E + \frac{\epsilon_0}{\alpha_L^2}(\epsilon_0 + \frac{1}{\alpha_\delta})T}\right)\right),$$
(19)

where $E_2 = O\left(\sum_{\tau=0}^{k-1} (R_0 \cdot q_1(\tau) + q_2(\tau)) \sum_{t=0}^{T} \rho_{p(t),\tau}^2 + (q_1(k)^2 + q_2(k)^2) T\right)$, p(t) denotes the last time step that plans before t.

D TECHNICAL PROOF

D.1 PROOF FOR MPC_k^m

Proof of Lemma C.1. Lemma 20 is a straight-forward implication of perturbation bound equation 10 To see this, for $t' = mn \le t < m(n+1)$, note that the per-step error e_t can be bounded by

$$e_{t|t'} = \left\| \psi_{t'}^{t'+k}(x_{t'}, \xi_{t':t'+k-1|t'}, \bar{y}(\xi_{t'+k|t'}); \mathbb{I})_{v_t} - \psi_t^T(x_t, \xi_{t:T}^*; F_T)_{v_t} \right\|$$

$$= \left\| \psi_{t'}^{t'+k}(x_{t'}, \xi_{t':t'+k-1|t'}, \bar{y}(\xi_{t'+k|t'}); \mathbb{I})_{v_t} - \psi_{t'}^{t'+k}(x_{t'}, \xi_{t':t'+k-1}^*, x_{t'+k|t'}^*; \mathbb{I})_{v_t} \right\|$$

$$\leq \sum_{\tau=0}^{k-1} \left(\|x_{t'}\| \cdot q_1(\tau) + q_2(\tau) \right) \rho_{t',\tau} + \left(\|x_{t'}\| \cdot q_1(k) + q_2(k) \right) \left\| \bar{y}(\xi_{t'+k|t'}) - x_{t'+k|t'}^* \right\|.$$
(20a)

Here, we apply the principle of optimality to conclude that the optimal trajectory from $x_{t'}$ to $x_{t'+k|t'}^*$ (i.e., $\psi_{t'}^{t'+k}(x_{t'}, \xi_{t':t'+k-1}^*, x_{t'+k|t'}^*; \mathbb{I})$ in equation 20b) is a sub-trajectory of the clairvoyant optimal trajectory from x_t (i.e., $\psi_t^T(x_t, \xi_{t:T}^*; F_T)$ in equation 20a), and equation 20c is obtained by directly applying perturbation bound equation 10. Note that $||x_{t'}|| \leq R_1 + D_{x^*}$, and that both $\bar{y}(\xi_{t'+k|t'})$ and $x_{t'+k|t'}^*$ are in $\mathcal{B}(x_{t+k}^*; R)$ by assumption and by perturbation bound equation 11 specified in Property C.1, we conclude that equation 13 hold for t < T - k. The case $t \geq T - k$ can be shown similarly.

Proof of Lemma C.2. We use mathematical induction to show how state deviations accumulate when executing multiple actions from a single plan. The key insight is that each action error compounds through the system dynamics.

We prove by induction for the first part. When t = t' + 1 (i.e., the first step after planning):

$$||x_{t'+1} - x_{t'+1|t'}^*|| = ||g_{t'}(x_{t'}, u_{t'}) - g_{t'}(x_{t'}, u_{t'|t'}^*)||$$

$$\leq L_{t'} ||u_{t'} - u_{t'|t'}^*||$$

$$\leq L_{t'} e_{t'|t'}.$$

Now suppose eq. (14) holds for t-1 (i.e., $\left\|x_t-x_{t-1|t'}^*\right\| \leq \sum_{\tau=t'}^{t-2} e_{\tau|t'} \prod_{s=\tau}^{t-2} L_s$). This means we assume the state deviation bound holds up to time t-1. We now show it holds for time t:

$$\begin{aligned} \left\| x_{t} - x_{t|t'}^{*} \right\| &= \left\| g_{t-1}(x_{t-1}, u_{t-1}) - g(x_{t-1|t'}^{*}, u_{t-1|t'}^{*}) \right\| \\ &\leq L_{t-1}(\left\| u_{t-1} - u_{t-1|t'}^{*} \right\| + (\left\| x_{t-1} - x_{t-1|t'}^{*} \right\|) \\ &\leq L_{t-1}e_{t-1|t'} + L_{t-1} \sum_{\tau=t'}^{t-2} e_{\tau|t'} \prod_{s=\tau}^{t-2} L_{s} \\ &= \sum_{\tau=t'}^{t-1} e_{\tau|t'} \prod_{s=\tau}^{t-1} L_{s} . \end{aligned}$$

Proof of Lemma C.3. First we bound $||x_t - x_t^*||$ and $||u_t - u_t^*||$

$$||x_{t} - x_{t}^{*}|| = ||x_{t} - x_{t|mn}^{*}|| + ||x_{t|mn}^{*} - x_{t}^{*}||$$

$$\leq ||x_{t} - x_{t|mn}^{*}|| + \sum_{i=0}^{n-1} ||x_{t|m(i+1)}^{*} - x_{t|mi}^{*}||$$

$$\leq ||x_{t} - x_{t|mn}^{*}|| + \sum_{i=0}^{n-1} q_{3}(t - (i+1)m) ||x_{m(i+1)} - x_{m(i+1)|mi}^{*}||$$

$$\leq \sum_{t=m}^{t-1} e_{\tau|mn} \prod_{t=0}^{t-1} L_{s} + \sum_{i=0}^{n-1} q_{3}(t - (i+1)m) \sum_{t=m}^{m(i+1)-1} e_{\tau|mi} \prod_{t=0}^{m(i+1)-1} L_{s}.$$

$$||u_{t} - u_{t}^{*}|| = ||u_{t} - u_{t|mn}^{*}|| + ||u_{t|mn}^{*} - u_{t}^{*}||$$

$$\leq ||u_{t} - u_{t|mn}^{*}|| + \sum_{i=0}^{n-1} ||u_{t|m(i+1)}^{*} - u_{t|mi}^{*}||$$

$$\leq ||u_{t} - u_{t|mn}^{*}|| + \sum_{i=0}^{n-1} q_{3}(t - (i+1)m) ||x_{m(i+1)} - x_{m(i+1)|mi}^{*}||$$

$$\leq e_{t|mn} + \sum_{i=0}^{n-1} q_{3}(t - (i+1)m) \sum_{\tau=mi}^{m(i+1)-1} e_{\tau|mi} \prod_{s=\tau}^{m(i+1)-1} L_{s}.$$

Without loss of generality, we define $q_3(k)=0$ for k<0. For simplicity of notation, we denote $L_*=\max_{0\leq t\leq T}\max_{0\leq i\leq m-1}\prod_{s=t}^{t+i}L_s$, which captures the maximum compounding effect of Lipschitz constants over m steps. So we arrive at

$$||x_t - x_t^*||, ||u_t - u_t^*|| \le L_* \sum_{i=0}^n q_3(t - (i+1)m) \sum_{\tau=m_i}^{m(i+1)-1} e_{\tau|m_i}.$$
 (21)

To bound the squared deviations (which will be needed for the cost analysis), we use the Cauchy-Schwarz inequality:

$$\begin{aligned} \|x_t - x_t^*\|^2 &\leq L_*^2 \left(\sum_{i=0}^n q_3(t - (i+1)m) \sum_{\tau=mi}^{m(i+1)-1} e_{\tau|mi} \right)^2 \\ &\leq L_*^2 \sum_{i=0}^n q_3(t - (i+1)m)) \left(\sum_{i=0}^n q_3(t - (i+1)m) \left(\sum_{\tau=mi}^{m(i+1)-1} e_{\tau|mi} \right)^2 \right) \\ &\leq m L_*^2 C_3 \left(\sum_{i=0}^n q_3(t - (i+1)m) \sum_{\tau=mi}^{m(i+1)-1} e_{\tau|mi}^2 \right) . \end{aligned}$$

This bound also holds for $||u_t - u_t^*||^2$, so we have

$$||x_t - x_t^*||^2 + ||u_t - u_t^*||^2 \le 2mL_*^2C_3 \left(\sum_{i=0}^n q_3(t - (i+1)m)\sum_{\tau=mi}^{m(i+1)-1} e_{\tau|mi}^2\right)$$

Without loss of generality, we assue T = Nm, we have

$$\sum_{t=1}^{T} \|x_{t} - x_{t}^{*}\|^{2} + \sum_{t=1}^{T} \|u_{t} - u_{t}^{*}\|^{2} \leq 2mL_{*}^{2}C_{3} \left(\sum_{n=0}^{N-1} \sum_{t=nm}^{(n+1)m-1} \sum_{i=0}^{n} q_{3}(t - (i+1)m) \sum_{\tau=mi}^{m(i+1)-1} e_{\tau|mi}^{2} \right) \\
\leq 2mL_{*}^{2}C_{3} \left(\sum_{i=0}^{N-1} \sum_{\tau=mi}^{m(i+1)-1} e_{\tau|mi}^{2} \sum_{n=i}^{N-1} \sum_{t=nm}^{(n+1)m-1} q_{3}(t - (i+1)m) \right) \\
\leq 2mL_{*}^{2}C_{3}^{2} \left(\sum_{i=0}^{N-1} \sum_{\tau=mi}^{m(i+1)-1} e_{\tau|mi}^{2} \right) \tag{22}$$

Since the cost function $f_t(\cdot,\cdot;\xi_t^*)$ and $F_T(\cdot;\xi_T^*)$ are nonnegative, convex, and ℓ -smooth in their inputs, by Lemma F.2 in Lin et al. (2021), we see that the following inequality holds for arbitrary $\eta>0$:

$$cost(ALG) - cost(OPT)
\leq \left(\sum_{t=0}^{T-1} f_t(x_t, u_t; \xi_t^*) + F_T(x_T; \xi_T^*) \right) - \left(\sum_{t=0}^{T-1} f_t(x_t^*, u_t^*; \xi_t^*) + F_T(x_T^*; \xi_T^*) \right)
\leq \eta \left(\sum_{t=0}^{T-1} f_t(x_t^*, u_t^*; \xi_t^*) + F_T(x_T^*; \xi_T^*) \right)
+ \frac{\ell}{2} \left(1 + \frac{1}{\eta} \right) \left(\sum_{t=1}^{T} \|x_t - x_t^*\|^2 + \sum_{t=0}^{T-1} \|u_t - u_t^*\|^2 \right)
\leq \eta \cdot cost(OPT) + \left(1 + \frac{1}{\eta} \right) \cdot \frac{\ell}{2} \cdot 2mL_*^2 C_3^2 \left(\sum_{i=0}^{N-1} \sum_{\tau=mi}^{m(i+1)-1} e_{\tau|mi}^2 \right)$$

$$= \eta \cdot cost(OPT) + \frac{1}{\eta} \cdot \frac{\ell}{2} \cdot 2mL_*^2 C_3^2 \left(\sum_{i=0}^{N-1} \sum_{\tau=mi}^{m(i+1)-1} e_{\tau|mi}^2 \right)$$

$$+ \frac{\ell}{2} \cdot 2mL_*^2 C_3^2 \left(\sum_{i=0}^{N-1} \sum_{\tau=mi}^{m(i+1)-1} e_{\tau|mi}^2 \right),$$
(23c)

where we apply Lemma F.2 in Lin et al. (2021) in equation 23a, and we use equation 22 in equation 23b. Setting the tunable weight η in equation 23c to be

$$\eta = \left(\frac{\frac{\ell}{2} \cdot 2mL_*^2 C_3^2 \left(\sum_{i=0}^{N-1} \sum_{\tau=mi}^{m(i+1)-1} e_{\tau|mi}^2\right)}{\text{cost}(\mathsf{OPT})}\right)^{\frac{1}{2}}$$

gives that

$$cost(ALG) - cost(OPT)
\leq \sqrt{\left(\frac{\ell}{2} \cdot 2mL_*^2 C_3^2\right) \cdot cost(OPT) \cdot \left(\sum_{i=0}^{N-1} \sum_{\tau=mi}^{m(i+1)-1} e_{\tau|mi}^2\right)}
+ \frac{\ell}{2} \cdot 2mL_*^2 C_3^2 \left(\sum_{i=0}^{N-1} \sum_{\tau=mi}^{m(i+1)-1} e_{\tau|mi}^2\right).$$
(24)

This finishes the proof.

Proof of Theorem C.4. We first use induction to show that the following two conditions holds for all time steps t < T:

$$x_t \in \mathcal{B}\left(x_t^*, R\right),\tag{25a}$$

$$e_{t|mn} \le \sum_{\tau=0}^{k} \left(\left(R_1 + D_{x^*} \right) \cdot q_1(\tau) + q_2(\tau) \right) \rho_{mn,\tau} + 2R_2 \left(\left(R_1 + D_{x^*} \right) \cdot q_1(k) + q_2(k) \right). \tag{25b}$$

At time step 0, equation 25a holds because $x_0 = x_0^*$, and equation 25b holds by lemma C.1 and the assumption on the terminal cost F_k of MPC_k.

Suppose equation 25a and equation 25b hold for all time steps $\tau < t$. For time step t, by the assumption on the prediction errors $\rho_{t,\tau}$ and prediction horizon k in Theorem C.4, we know that $e_{\tau} \leq \frac{R}{C_3^2 L_g}$ holds for all $\tau < t$ because equation 25b holds for all $\tau < t$. Thus, we know that equation 25a holds for time step t by Equation (21) since

$$||x_t - x_t^*|| \le L_* \sum_{i=0}^n q_3(t - (i+1)m) \sum_{\tau=mi}^{m(i+1)-1} e_{\tau|mi}$$

$$\le mL_* \frac{R_1}{mC_3L_*} \sum_{i=0}^n q_3(t - (i+1)m)$$

$$\le \frac{R_1}{C_2} \cdot C_3 = R_1$$

Then, since equation 25a holds for time step t, and the terminal cost F_{t+k} of MPC $_k$ is set to be the indicator function of some state $\bar{y}(\xi_{t+k|t})$ that satisfies $\bar{y}(\xi_{t+k|t}) \in \mathcal{B}(x_{t+k}^*, R_1)$ if t < T - k, we know equation 25b also holds for time step t by Lemma C.1. This finishes the induction proof of equation 25.

To simplify the notation, let $R_0 := R_1 + D_{x^*}$. Note that equation 25b implies that

$$e_{t|mn}^{2} \leq \left(\sum_{\tau=0}^{k} \left(R_{0} \cdot q_{1}(\tau) + q_{2}(\tau)\right) + 2R_{2}\left(R_{0} + 1\right)\right)$$

$$\cdot \left(\sum_{\tau=0}^{k} \left(R_{0} \cdot q_{1}(\tau) + q_{2}(\tau)\right) \rho_{mn,\tau}^{2} + 2R_{2}\left(R_{0} \cdot q_{1}(k)^{2} + q_{2}(k)^{2}\right)\right)$$

$$\leq \left(R_{0}C_{1} + C_{2} + 2R_{2}(R_{0} + 1)\right)$$

$$\cdot \left(\sum_{\tau=0}^{k-1} \left(R_{0} \cdot q_{1}(\tau) + q_{2}(\tau)\right) \rho_{mn,\tau}^{2} + \left(2R_{2} + 1\right) \left(R_{0} \cdot q_{1}(k)^{2} + q_{2}(k)^{2}\right)\right), \quad (26b)$$

where we use the Cauchy-Schwarz inequality in equation 26a; we use the bounds $\sum_{\tau=0}^{k} q_1(\tau) \leq C_1$ and $\sum_{\tau=0}^{k} q_2(\tau) \leq C_2$ in equation 26b.

1175
1176
1177
$$\sum_{n=0}^{N} \sum_{t=mn}^{m(n-1)-1} e_{t|mn}^{2} \qquad (27a)$$
1179
$$\leq (R_{0}C_{1} + C_{2} + 2R_{2}(R_{0} + 1))$$
1180
$$\cdot \left(\sum_{\tau=0}^{k-1} (R_{0} \cdot q_{1}(\tau) + q_{2}(\tau)) \sum_{n=0}^{N} \sum_{t=mn}^{m(n-1)-1} \rho_{mn,\tau}^{2} + (2R_{2} + 1) \left(R_{0} \cdot q_{1}(k)^{2} + q_{2}(k)^{2}\right) T\right)$$
1183
$$\leq (R_{0}C_{1} + C_{2} + 2R_{2}(R_{0} + 1))$$
1184
$$\leq (R_{0}C_{1} + C_{2} + 2R_{2}(R_{0} + 1))$$
1186
$$\cdot \left(\sum_{t=0}^{k-1} (R_{0} \cdot q_{1}(\tau) + q_{2}(\tau)) \sum_{t=0}^{N} m\rho_{mn,\tau}^{2} + (2R_{2} + 1) \left(R_{0} \cdot q_{1}(k)^{2} + q_{2}(k)^{2}\right) T\right)$$
(27c)

Since equation 25 and equation 29 holds for all time steps t < T, we can apply Lemma C.3 to obtain that

$$cost(\mathsf{MPC}_k^m) - cost(\mathsf{OPT}) = O\left(mL_*^2\sqrt{cost(\mathsf{OPT})\cdot E_1} + mL_*^2E_1\right) ,$$

where

$$E_1 := \left(R_0 C_1 + C_2 + 2R_2 (R_0 + 1) \right) \cdot \left(\sum_{\tau=0}^{k-1} \left(R_0 \cdot q_1(\tau) + q_2(\tau) \right) \sum_{n=0}^{N} m \rho_{mn,\tau}^2 + \left(2R_2 + 1 \right) \left(R_0 \cdot q_1(k)^2 + q_2(k)^2 \right) T \right)$$

This finishes the proof of Theorem C.4.

D.2 PROOF FOR $MPC_{k,\epsilon}$

Proof of Lemma C.5. We bound the per-step error by decomposing it into two parts: the error due to state deviation from the planned trajectory, and the error due to parameter uncertainty.

Let $\hat{x}_{t|t'} := \psi_{t'}^{t'+k}(x_{t'}, \xi_{t':t'+k-1|t'}, \bar{y}(\xi_{t'+k|t'})_{y_t}$ be the planned state at time t from the plan computed at time t'. We have

$$e_{t} = \left\| \psi_{t'}^{t'+k}(x_{t'}, \xi_{t':t'+k-1|t}, \bar{y}(\xi_{t'+k|t'}); \mathbb{I})_{v_{t}} - \psi_{t}^{T}(x_{t}, \xi_{t:T}^{*}; F_{T})_{v_{t}} \right\|$$

$$= \left\| \psi_{t}^{t'+k}(\hat{x}_{t|t'}, \xi_{t:t'+k-1|t'}, \bar{y}(\xi_{t'+k|t}); \mathbb{I})_{v_{t}} - \psi_{t}^{t'+k}(x_{t}, \xi_{t:t'+k-1}^{*}, x_{t'+k|t}^{*}; \mathbb{I})_{v_{t}} \right\|$$

$$\leq \left\| \psi_{t}^{t'+k}(\hat{x}_{t|t'}, \xi_{t:t'+k-1|t'}, \bar{y}(\xi_{t'+k|t'}); \mathbb{I})_{v_{t}} - \psi_{t}^{t'+k}(x_{t}, \xi_{t:t'+k-1|t'}, \bar{y}(\xi_{t'+k|t'}); \mathbb{I})_{v_{t}} \right\|$$

$$+ \left\| \psi_{t}^{t'+k}(x_{t}, \xi_{t:t'+k-1|t'}, \bar{y}(\xi_{t'+k|t'}); \mathbb{I})_{v_{t}} - \psi_{t}^{t'+k}(x_{t}, \xi_{t:t'+k-1}^{*}, x_{t+k|t}^{*}; \mathbb{I})_{v_{t}} \right\|$$

$$\leq q_{3}(0) \left\| \hat{x}_{t|t'} - x_{t} \right\|$$

$$\leq q_{3}(0) \left\| \hat{x}_{t|t'} - x_{t} \right\|$$

$$+ \sum_{\tau=t-t'} \left(\left\| x_{t} \right\| \cdot q_{1}(\tau) + q_{2}(\tau) \right) \rho_{t',\tau} + \left(\left\| x_{t} \right\| \cdot q_{1}(k) + q_{2}(k) \right) \left\| \bar{y}(\xi_{t+k|t}) - x_{t+k|t}^{*} \right\|$$

$$(28b)$$

$$\leq q_3(0)\epsilon + \sum_{\tau=0}^{k-1} \left((D_{x^*} + R_1) \cdot q_1(\tau) + q_2(\tau) \right) \rho_{t',\tau} + 2R_2 \left(\|x_t\| \cdot q_1(k) + q_2(k) \right). \tag{28d}$$

In equation 28a, we use the fact that the imagined optimal trajectory starting from imagined state $\hat{x}_{t|t'}$ (i.e. $\psi_t^{t'+k}(\hat{x}_{t|t'}, \xi_{t:t'+k-1|t'}, \bar{y}(\xi_{t'+k|t}); \mathbb{I})_{y_{t:t'+k}, v_{t:t'+k}})$ is sub-trajectory of the imagined optimal trajectory starting from state $x_{t'}$ (i.e. $\psi_{t'}^{t'+k}(x_{t'}, \xi_{t':t'+k-1|t}, \bar{y}(\xi_{t'+k|t'}); \mathbb{I})_{y_{t':t'+k}, v_{t':t'+k}})$. In equation 28b we apply perturbation bound equation 10 and in equation 28c we apply perturbation bound equation 11. Equation (28d) comes from the assumption that $x_t \in \mathcal{B}(x_t^*, R_1)$.

Proof of Theorem C.6. This proof is a simple extension of the proof of Theorem C.4 and Theorem 3.3 in (Lin et al., 2022).

By Lemma 3.2 in (Lin et al., 2022), we have

$$||x_t - x_t^*|| \le L \sum_{i=0}^{t-1} q_3(i) e_{t-i-1} \le L \cdot \frac{R_1}{C_3 L} \sum_{i=0}^{t-1} q_3(i) \le R_1.$$

With the same induction as Theorem C.4 we can see $x_t \in \mathcal{B}(x_t^*, R_1)$ so the perturbation bounds hold.

To simplify the notation, let $R_0 := R_1 + D_{x^*}$. Note that equation 17 implies that

$$\begin{aligned} & 2244 & e_t^2 \leq \left(q_3(0)\epsilon\right)^2 \\ & + \left(\sum_{\tau=0}^k \left(R_0 \cdot q_1(\tau) + q_2(\tau)\right) \rho_{p(t),\tau} + 2R_2 \left(R_0 \cdot q_1(k) + q_2(k)\right)\right)^2 \\ & + 2q_3(0)\epsilon \left(\sum_{\tau=0}^k \left(R_0 \cdot q_1(\tau) + q_2(\tau)\right) \rho_{p(t),\tau} + 2R_2 \left(R_0 \cdot q_1(k) + q_2(k)\right)\right) \\ & \leq q_3(0)^2 \epsilon^2 \\ & + \left(\sum_{\tau=0}^k \left(R_0 \cdot q_1(\tau) + q_2(\tau)\right) + 2R_2 \left(R_0 + 1\right)\right) \\ & \cdot \left(\sum_{\tau=0}^k \left(R_0 \cdot q_1(\tau) + q_2(\tau)\right) \rho_{p(t),\tau}^2 + 2R_2 \left(R_0 \cdot q_1(k)^2 + q_2(k)^2\right)\right) \\ & + 2q_3(0)\epsilon \left(\sum_{\tau=0}^k \left(R_0 \cdot q_1(\tau) + q_2(\tau)\right) \rho_{p(t),\tau} + 2R_2 \left(R_0 \cdot q_1(k) + q_2(k)\right)\right) \\ & + 2q_3(0)\epsilon \left(\sum_{\tau=0}^k \left(R_0 \cdot q_1(\tau) + q_2(\tau)\right) \rho_{p(t),\tau} + 2R_2 \left(R_0 \cdot q_1(k) + q_2(k)\right)\right) \\ & \leq O\left(\epsilon^2 + \epsilon \left(\sum_{\tau=0}^k \left(R_0 \cdot q_1(\tau) + q_2(\tau)\right) \rho_{p(t),\tau} + 2R_2 \left(R_0 \cdot q_1(k) + q_2(k)\right)\right) \\ & + O\left(R_0C_1 + C_2 + 2R_2(R_0 + 1)\right) \\ & \cdot \left(\sum_{\tau=0}^{k-1} \left(R_0 \cdot q_1(\tau) + q_2(\tau)\right) \rho_{p(t),\tau}^2 + \left(2R_2 + 1\right) \left(R_0 \cdot q_1(k)^2 + q_2(k)^2\right)\right), \end{aligned} \tag{29c}$$

where p(t) denotes the last time step that plans before t. We use the Cauchy-Schwarz inequality in equation 29b; we use the bounds $\sum_{\tau=0}^{k} q_1(\tau) \leq C_1$, $\sum_{\tau=0}^{k} q_2(\tau) \leq C_2$ in equation 29c.

Finally, we apply Lemma 3.2 in (Lin et al., 2022) and Lemma F.2 in Lin et al. (2021) to connect the per-step errors to overall performance:

$$\begin{split} & \operatorname{cost}(\mathsf{MPC}_{k,\epsilon}) - \operatorname{cost}(\mathsf{OPT}) \\ & \leq \sqrt{\left(\frac{\ell}{2} \cdot (1 + 2C_3L^2) \cdot (1 + C_3)\right) \cdot \operatorname{cost}(\mathsf{OPT}) \cdot \sum_{t=0}^{T-1} e_t^2} \\ & + \frac{\ell}{2} \cdot \left(1 + 2C_3L^2\right) \cdot (1 + C_3) \cdot \sum_{t=0}^{T-1} e_t^2. \\ & = O\left(\sqrt{L^2 \mathrm{cost}(\mathsf{OPT}) \cdot (E_2 + + \epsilon E + \epsilon^2 T)} + L^2(E_2 + \epsilon E + \epsilon^2 T)\right) \;, \end{split} \tag{30a}$$

where

$$E_2 := \left(R_0 C_1 + C_2 + 2R_2 (R_0 + 1) \right) \cdot \left(\sum_{\tau=0}^{k-1} \left(R_0 \cdot q_1(\tau) + q_2(\tau) \right) \sum_{t=0}^{T} \rho_{p(t),\tau}^2 + \left(2R_2 + 1 \right) \left(R_0 \cdot q_1(k)^2 + q_2(k)^2 \right) T \right).$$

D.3 PROOF FOR MPC $_{AB}$

Proof. We extend the analysis of MPC_{k, ϵ} to handle time-varying thresholds. The key insight is that our adaptive threshold choice allows us to bound the additional regret terms more tightly.

 First we introduce an adaptation of Equation (29) for time-varying thresholds.

$$\begin{aligned} & \text{1299} \\ & \text{1300} \\ & e_t^2 \leq \left(q_3(0)\epsilon_t + \sum_{\tau=0}^k \left(R_0 \cdot q_1(\tau) + q_2(\tau)\right)\rho_{p(t),\tau} + 2R_2\left(R_0 \cdot q_1(k) + q_2(k)\right)\right)^2 \\ & \text{1301} \\ & \text{1302} \\ & \text{1303} \\ & \leq \left(q_3(0)^2\epsilon_t + \sum_{\tau=0}^k \left(R_0 \cdot q_1(\tau) + q_2(\tau)\right) + 2R_2\left(R_0 + 1\right)\right) \\ & \cdot \left(\epsilon_t + \sum_{\tau=0}^k \left(R_0 \cdot q_1(\tau) + q_2(\tau)\right)\rho_{p(t),\tau}^2 + 2R_2\left(R_0 \cdot q_1(k)^2 + q_2(k)^2\right)\right) \\ & \text{1306} \\ & \text{1307} \\ & \leq \left(R_0C_1 + C_2 + 2R_2(R_0 + 1)\right) \\ & \text{1308} \\ & \text{1310} \\ & \text{1310} \\ & \text{1311} \\ & \text{1312} \\ & \text{1313} \\ & + O\left(\epsilon_t^2 + \epsilon_t \left(\sum_{\tau=0}^{k-1} \left(R_0 \cdot q_1(\tau) + q_2(\tau)\right)\rho_{p(t),\tau}^2 + \left(2R_2 + 1\right)\left(R_0 \cdot q_1(k)^2 + q_2(k)^2\right)\right)\right), \\ & \text{1314} \\ & \text{1315} \end{aligned}$$

where we use Cauchy-Schwarz inequality in Equation (31b).

Then we bound $||x_t - x_t^*||$ in a more fine-grained way to account for the adaptive nature of our algorithm:

$$||x_{t} - x_{t}^{*}|| = ||x_{t} - \psi_{0}^{T}(x_{0})_{y_{t}}||$$

$$\leq ||x_{t} - \psi_{t-1}^{T}(x_{t-1})_{y_{t}}|| + \sum_{i=1}^{t-1} ||\psi_{t-i}^{T}(x_{t-i})_{y_{t}} - \psi_{t-i-1}^{T}(x_{t-i-1})_{y_{t}}||$$

$$\leq ||x_{t} - \psi_{t-1}^{T}(x_{t-1})_{y_{t}}|| + \sum_{i=1}^{t-1} q_{3}(i) ||x_{t-i} - \psi_{t-i-1}^{T}(x_{t-i-1})_{y_{t-i}}||$$

$$\leq \sum_{i=0}^{t-1} q_{3}(i) ||x_{t-i} - \psi_{t-i-1}^{T}(x_{t-i-1})_{y_{t-i}}||$$

$$\leq \sum_{i=0}^{t-1} q_{3}(i) L_{t-i-1}e_{t-i-1},$$

$$(34)$$

Taking squares and applying Cauchy-Schwarz:

$$||x_{t} - x_{t}^{*}||^{2} \leq \left(\sum_{i=0}^{t-1} q_{3}(i) L_{t-i-1} e_{t-i-1}\right)^{2}$$

$$\leq \left(\sum_{i=0}^{t-1} q_{3}(i)\right) \cdot \left(\sum_{i=0}^{t-1} q_{3}(i) L_{t-i-1}^{2} e_{t-i-1}^{2}\right)$$

$$\leq C_{3} \left(\sum_{i=0}^{t-1} q_{3}(i) L_{t-i-1}^{2} e_{t-i-1}^{2}\right). \tag{35a}$$

Similarly, we can bound the control deviations:

$$||u_{t} - u_{t}^{*}||^{2} \leq \left(e_{t} + \sum_{i=0}^{t-1} q_{3}(i) L_{t-i-1} e_{t-i-1}\right)^{2}$$

$$\leq \left(1 + \sum_{i=0}^{t-1} q_{3}(i)\right) \cdot \left(e_{t}^{2} + \sum_{i=0}^{t-1} q_{3}(i) L_{t-i-1}^{2} e_{t-i-1}^{2}\right)$$
(36a)

$$\leq (1 + C_3) \cdot \left(\sum_{i=0}^{t} q_3(i) L_{t-i-1}^2 e_{t-i-1}^2\right),$$
 (36b)

Summing equation 35 and equation 36 over time steps t gives that

$$\sum_{t=1}^{T} \|x_t - x_t^*\|^2 + \sum_{t=0}^{T-1} \|u_t - u_t^*\|^2
\leq C_3 \sum_{t=1}^{T} \left(\sum_{i=0}^{t-1} q_3(i) L_{t-i-1}^2 e_{t-i-1}^2 \right) + (1 + C_3) \cdot \sum_{t=0}^{T-1} \left(\sum_{i=0}^{t-1} q_3(i) L_{t-i-1}^2 e_{t-i-1}^2 \right)
\leq (1 + 2C_3) \sum_{t=0}^{T-1} L_t^2 e_t^2,$$
(37)

where we rearrange the terms and use $\sum_{j=0}^{\infty} q_3(j) \leq C_3$ in the last inequality.

By Lemma F.2 in Lin et al. (2021) with similar analysis in previous theorem, we arrive at

$$\begin{split} & \operatorname{cost}(\mathsf{MPC}_{k,\epsilon}) - \operatorname{cost}(\mathsf{OPT}) \\ & \leq \sqrt{\left(\frac{\ell}{2} \cdot (1 + 2C_3)\right) \cdot \operatorname{cost}(\mathsf{OPT}) \cdot \sum_{t=0}^{T-1} L_t^2 e_t^2} + \frac{\ell}{2} \cdot (1 + 2C_3) \cdot \sum_{t=0}^{T-1} L_t^2 e_t^2 \;. \end{split}$$

Now we focus on $L_t^2 e_t^2$ and the three terms in Equation (31c). The first term corresponds to the regret of standard MPC_k. The second term captures the effect of our adaptive threshold, which we show is well-controlled. To see this, we have

$$L_t \epsilon_t \le \epsilon_0 L_t \exp(-\alpha_L \widehat{L}_t) \le \epsilon_0 \frac{L_t}{e \cdot \alpha_L \cdot \widehat{L}_t} \le \epsilon_0 \frac{L_t}{e \cdot \alpha_L \cdot \lambda L_t} = \frac{\epsilon_0}{e \lambda \alpha_L} , \qquad (38a)$$

where we use the inequality $\exp(-x) \le \frac{1}{ex}$ for x>0 in the second step. This gives us

$$L_t^2 \epsilon_t^2 \le \frac{\epsilon_0^2}{e^2 \lambda^2 \alpha_L^2} \ . \tag{38b}$$

For the third term, we denote $s_t := \sum_{\tau=0}^{k-1} \left(R_0 \cdot q_1(\tau) + q_2(\tau)\right) \rho_{p(t),\tau}^2 + (2R_2 + 1) \left(R_0 \cdot q_1(k)^2 + q_2(k)^2\right)$ for the simplicity of notation, thus

$$L_t^2 \epsilon_t s_t \le \epsilon_0 \cdot \left(L_t^2 \exp(-\alpha_L L_t) \right) \cdot \left(\exp(-\alpha_\delta \delta_t^o) s_t \right) \tag{38c}$$

$$\leq \epsilon_0 \cdot \left(\frac{4L_t^2}{e^2 \alpha_t^2 \widehat{L}_t^2} \right) \cdot \left(\frac{s_t}{e \alpha_\delta \delta_t^o} \right)$$
(38d)

$$\leq \epsilon_0 \cdot \left(\frac{4}{e^2 \alpha_T^2 \lambda^2}\right) \cdot \left(\frac{1}{e \alpha_\delta \mu}\right) = \frac{4\epsilon_0}{e^3 \lambda^2 \mu \alpha_T^2 \alpha_\delta} ,$$
(38e)

where we use the fact that $\exp(-x) \le \frac{1}{ex}$ and $\exp(-x) \le \frac{4}{e^2x^2}$ in the second inequality. Combining everything together, we have our final regret bound

$$\begin{split} & \cos (\mathsf{MPC}_{k,\epsilon}) - \cos (\mathsf{OPT}) \\ & \leq O\left(\sqrt{\cos (\mathsf{OPT})(L^2E + \frac{\epsilon_0}{\alpha_L^2}(\epsilon_0 + \frac{1}{\alpha_\delta})T)} + L^2E + \frac{\epsilon_0}{\alpha_L^2}(\epsilon_0 + \frac{1}{\alpha_\delta})T\right) \,. \end{split}$$

where

$$E_2 := \left(R_0 C_1 + C_2 + 2R_2 (R_0 + 1) \right) \cdot \left(\sum_{\tau=0}^{k-1} \left(R_0 \cdot q_1(\tau) + q_2(\tau) \right) \sum_{t=0}^{T} \rho_{p(t),\tau}^2 + \left(2R_2 + 1 \right) \left(R_0 \cdot q_1(k)^2 + q_2(k)^2 \right) T \right).$$

The above result may not recover to previous results when $\alpha_L=\alpha_\delta=0$. To mitigate this, we not need to apply the inequality $\exp(-x)\leq \frac{1}{1+x^2}$ and $\exp(-x)\leq \frac{1}{1+x^2}$ in Equation (38a) and Equation (38d) when x are extremely small. So it can still be proved that the regret of MPC_{AR} is no more than regret of $\mathsf{MPC}_{k,\varepsilon}$

E EXPERIMENT DETAILS

This appendix provides further details on the experimental setup described in Section 4.

E.1 SIMULATED EXPERIMENTS SETUP

Simulated experiments in this work are conducted on the VP2 Tian et al. (2023b) benchmark. All experiments can be conducted on a single NVIDIA GeForce RTX 4090 GPU. For each run of the experiments, it takes approximately 2500-3000 MiB of GPU memory for video prediction models like SVG (Villegas et al., 2019) and Struct-VRNN (Minderer et al., 2019). The simulator models and associated processes typically consume 20-25 GB of CPU RAM. Evaluating one learned model on a single task for one seed takes approximately 0.5-1 hour, while evaluations involving direct interaction with the simulator models (including noisy simulators in Appendix E.6 and visual vorrupted simulators in Appendix E.7) can take 2-3 hours per task per seed due to potentially different computational characteristics.

E.2 REAL-WORLD EXPERIMENTS SETUP

As shown in Figure 9, our real-world experiments are conducted using a Franka Emika Panda robotic arm. The arm is equipped with a simple cubic pusher as its end-effector to interact with the environment and objects. To obtain precise and high-frequency measurements of the keypoints defining the state , we utilize a Vicon motion capture system. This system provides accurate 3D coordinate data, which forms the basis for the state representations x_t used by our learned world models and the MPC controller in the real-world tasks.

E.3 STATE-BASED WORLD MODELING FOR REAL-WORLD TASKS

For the real-world experiments utilizing state-based representations (as opposed to vision-based models used in simulation), we learn task-specific, single-step dynamics models f. These models predict the next state x_{t+1} given the current state x_t and the action u_t applied by the robot's end-effector (pusher):

$$x_{t+1} = f(x_t, u_t) . (39)$$

Here, $u_t \in \mathbb{R}^2$ typically represents the 2D movement command sent to the end-effector. The specific state representation $x \in \mathbb{R}^d$ varies depending on the task:

• Open Door Task: The state $x \in \mathbb{R}^6$ comprises the 2D coordinates of the door hinge (axis) (x_0, y_0) , the door handle/endpoint (x_1, y_1) , and the robot end-effector (pusher) (x_e, y_e) , as

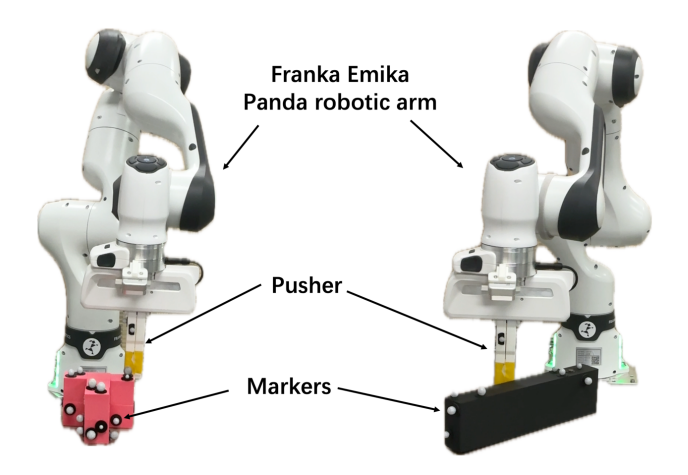
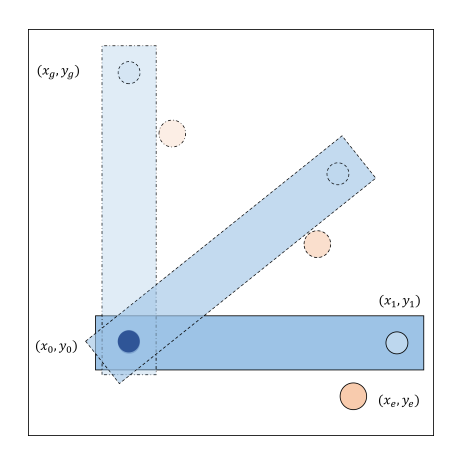
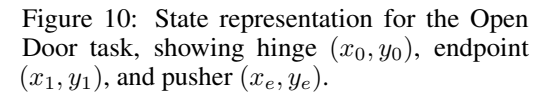


Figure 9: Real-World Experiments Setup

illustrated in Figure 10. Note that while the hinge position (x_0, y_0) is fixed during any single task execution trial, its location may vary across different trials in the data collection phase. This variation encourages the learned model f to generalize to different initial door configurations. We utilize classical 3 layer MLP model structure.

• Push T-Block Task: The state $x \in \mathbb{R}^8$ includes the 2D coordinates of three key points defining the T-block's pose (e.g., top-left (x_1,y_1) , top-right (x_2,y_2) , and bottom-middle (x_3,y_3)), along with the end-effector coordinates (x_e,y_e) , illustrated in Figure 11. These points allow tracking the object's position and orientation. We utilize classical 6 layer MLP model structure.





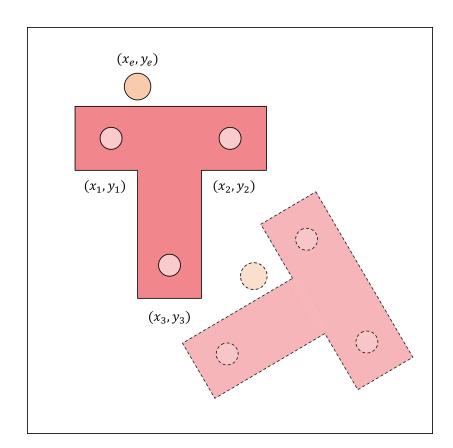


Figure 11: State representation for the Push T-Block task, showing key points (x_1, y_1) , (x_2, y_2) , (x_3, y_3) and pusher (x_e, y_e) .

E.4 DATA COLLECTION FOR STATE-BASED MODELS

For each task setting requiring a state-based model, training data for the dynamics model f (Eq. equation $\ref{eq:condition}$) was collected from two primary sources:

1. **Expert Demonstrations:** A collection of successful task executions providing examples of effective interactions. Demonstrations were gathered via human teleoperation and potentially supplemented by trajectories generated using path planning algorithms (like RRT) to reach specific target configurations.

2. **Random Exploration:** Data gathered from trajectories generated by applying random actions within the operational workspace. This source contributes a significant portion of the dataset to ensure broad coverage.

Combining targeted expert data with broad exploration data aims to prevent the model f from overfitting to specific demonstration trajectories. This strategy helps ensure the model captures dynamics across a wider range of the state-action space, potentially improving prediction accuracy along near-optimal paths discovered during online planning.

E.5 WORLD MODEL TRAINING

 The learned world models are trained as one-step predictors. For models trained from scratch (e.g., state-based models), we used the Adam optimizer with a learning rate of 5×10^{-6} and a batch size of 16. These models were trained for a total of 300 epochs. During the inference phase for planning, multi-step future predictions are generated by recursively applying the learned one-step predictor. Specifically, to predict k future steps given a sequence of actions from time t to t+k-1, the model autoregressively predicts $x_{t+1}, x_{t+2}, \ldots, x_{t+k}$.

E.6 Details for Disturbed Simulators as World Model

We add gaussian noise with mean 0 and different std for different components with various disturbance level to construct noisy simulator, with details summarized in Table 3.

Table 3: Standard deviations (std) of Gaussian noise applied to state components for different disturbance levels in the noisy simulator experiments.

| | Level 1 | Level 2 | Level 3 |
|-----------------------|---------|---------|---------|
| robot position | 0.001 | 0.005 | 0.010 |
| robot velocity | 0.001 | 0.005 | 0.010 |
| object position | 0.000 | 0.001 | 0.005 |
| object velocity | 0.000 | 0.001 | 0.005 |
| end effector position | 0.001 | 0.005 | 0.010 |

E.7 DETAILS FOR VISUAL CORRUPTED SIMULATORS AS WORLD MODEL

To assess the impact of imperfect visual predictions from a world model (distinct from errors in an underlying state representation), we apply two types of visual corruption to the images generated by an otherwise accurate simulator before they are processed (e.g., by a feature extractor like DINO):

- Gaussian Noise: Additive Gaussian noise is applied directly to the pixel values of the predicted images to make them appear more noisy.
- 2. **Gaussian Blur:** A Gaussian filter is applied to the predicted images to make them appear more blurry.

The parameters for these visual corruptions are detailed in Tables 4 and 5 and visualizations are in Figures 12 and 13.

Table 4: Parameters for adding Gaussian noise to predicted images. 'std' refers to the standard deviation of the noise.

| Noise Level | std |
|-------------|-----|
| Level 1 | 0.1 |
| Level 2 | 0.2 |
| Level 3 | 0.5 |
| | |

Table 5: Parameters for applying Gaussian blur to predicted images. 'sigma' refers to the standard deviation (kernel size) of the Gaussian filter.

| Blurriness Level | sigma |
|------------------|-------|
| Level 1 | 0.1 |
| Level 2 | 0.5 |
| Level 3 | 1.0 |



Figure 12: Visualization of different Noise Levels.

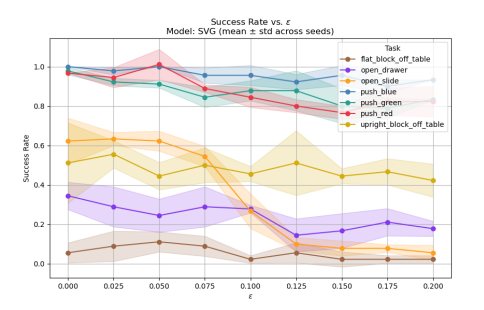


Figure 13: Visualization of different Blurriness Levels.

F MORE EXPERIMENTAL RESULTS

F.1 EXPERIMENTAL RESULTS FOR MPC_k^m AND $MPC_{k,\epsilon}$

We first explore how fixed m (number of steps to execute per plan) and ϵ (deviation threshold for replanning) influence the performance (success rate) and computational cost (NFE) of world model planning in simulation. This provides baseline intuition for understanding the trade-offs involved and motivates the need for adaptive approaches. The results are presented for the SVG and Struct-VRNN models on the VP2 benchmark tasks.



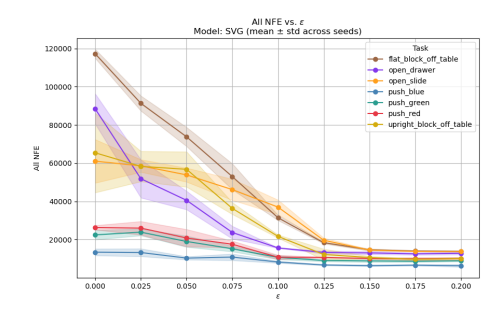
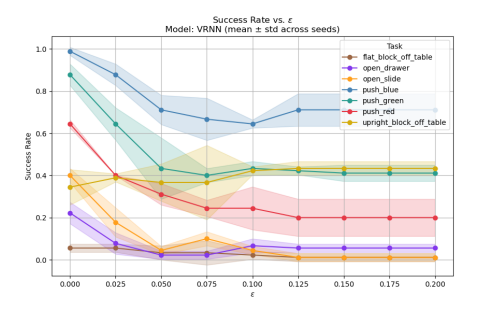


Figure 14: Performance of SVG model with MPC $_{k,\epsilon}$ for different deviation thresholds ϵ .



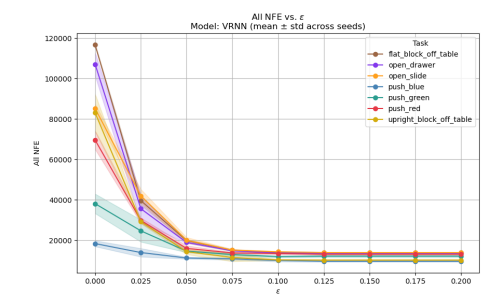


Figure 15: Performance of Struct-VRNN model with MPC_{k, ϵ} for different deviation thresholds ϵ .

As our theoretical analysis suggests (Section 3.1), both task performance (success rate) and computational cost (NFE) tend to decrease as m (number of steps per plan) and ϵ (replanning threshold) increase. However, the rate at which performance degrades varies significantly. This variation is influenced by factors such as the prediction quality of the specific world model and the sensitivity of the local dynamics encountered along the trajectories across different tasks. These results highlight the challenge of selecting a single fixed m or ϵ that performs optimally across all scenarios, motivating our adaptive approach.

F.2 TRAJECTORY VISUALIZATION OF REAL-WORLD EXPERIMENTS

The trajectory visualizations of our real-world experiments, presented in Figures 18 to 22, demonstrate the significant advantages of our adaptive replanning algorithm (ADAREP). These figures qualitatively

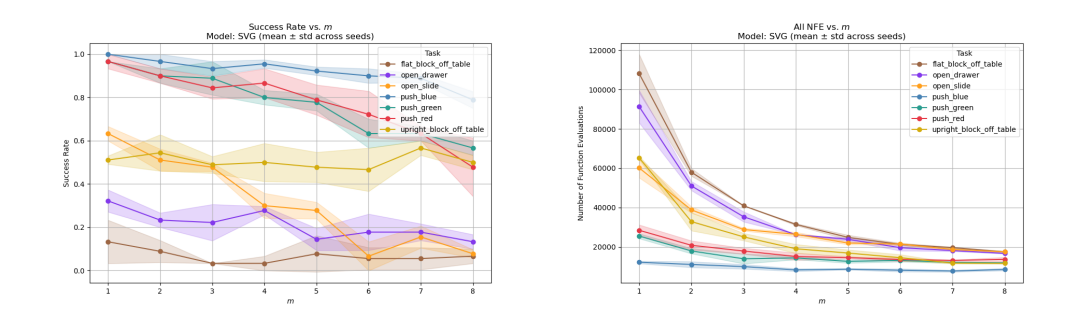


Figure 16: Performance of SVG model with MPC $_k^m$ for different numbers of executed steps m.

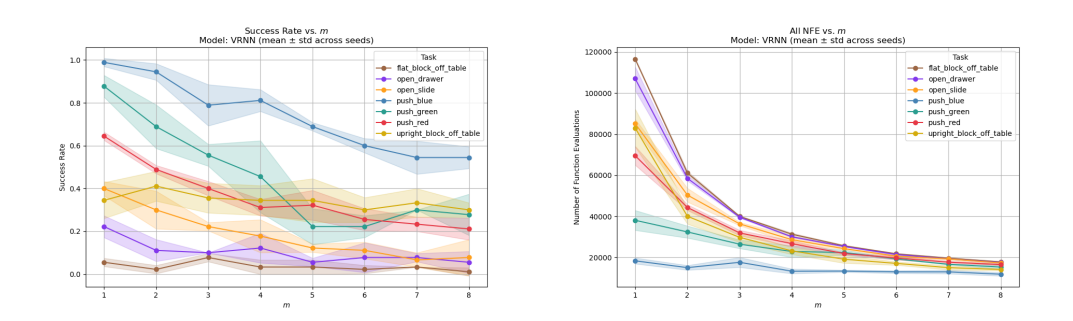


Figure 17: Performance of Struct-VRNN model with MPC_k^m for different numbers of executed steps m.

compare the behavior of ADAREP against the baseline MPC_k^1 . Different colors along an agent's path indicate segments executed from distinct plans; consequently, fewer color changes in the trajectories generated by ADAREP visually highlight its reduced replanning frequency and the associated computational savings.

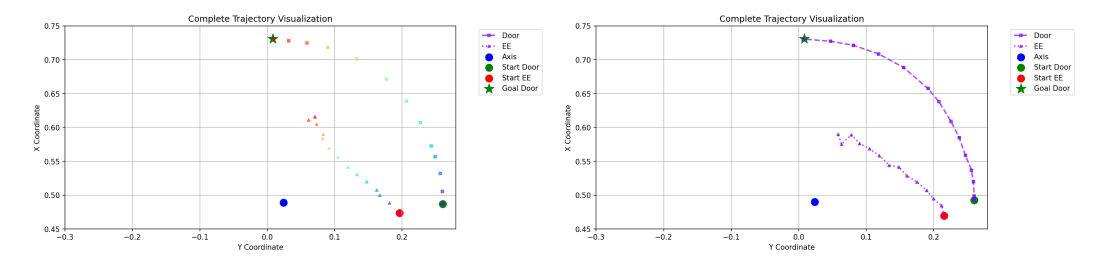


Figure 18: Trajectory of opening door to 90° . Left: MPC_k. Right: MPC_{AR}.

G MORE ANALYSIS AND DISCUSSIONS

ADAREP does require additional hyperparameter tuning, how ever we clarify that the tuning for ADAREP is a modest, one-time, upfront cost that yields substantial, continuous benefits.

Our tuning process is efficient as it builds upon the baseline. A practitioner can start with a reasonable fixed threshold ϵ and then simply tune ADAREP's parameters , which intuitively control the adaptation's sensitivity. This is significantly faster than exhaustively searching for the "perfect".

We want to further demonstrate that both our adaptive method (ADAREP) and other non-adaptive method (MPC $_k^m$, MPC $_{k,\epsilon}$) rely on hyperparameter tuning, adaptive method is indeed much better.

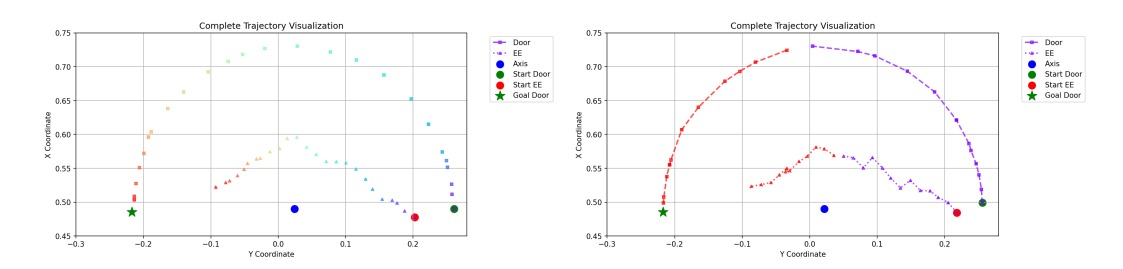


Figure 19: Trajectory of opening door to 180° . Left: MPC_k. Right: MPC_{AR}. Different colors represent controls from different plans.

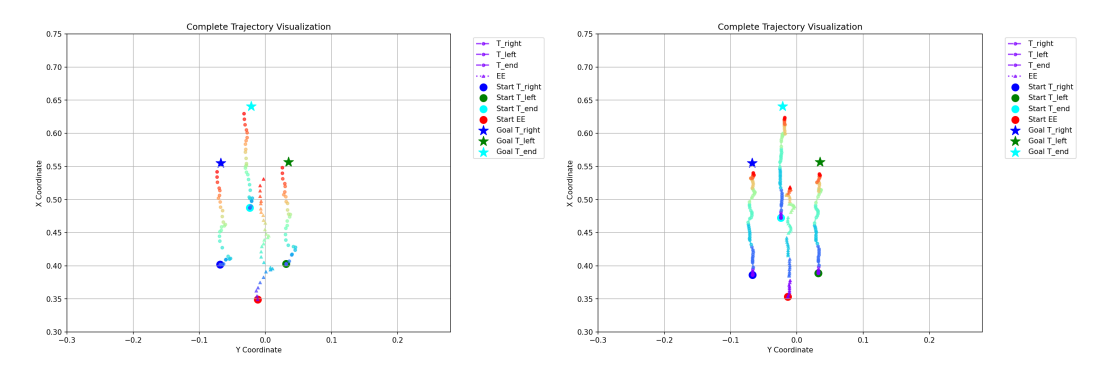


Figure 20: Trajectory of translating T-block. Left: MPC_k^1 . Right: MPC_{AR} . Different colors represent controls from different plans.

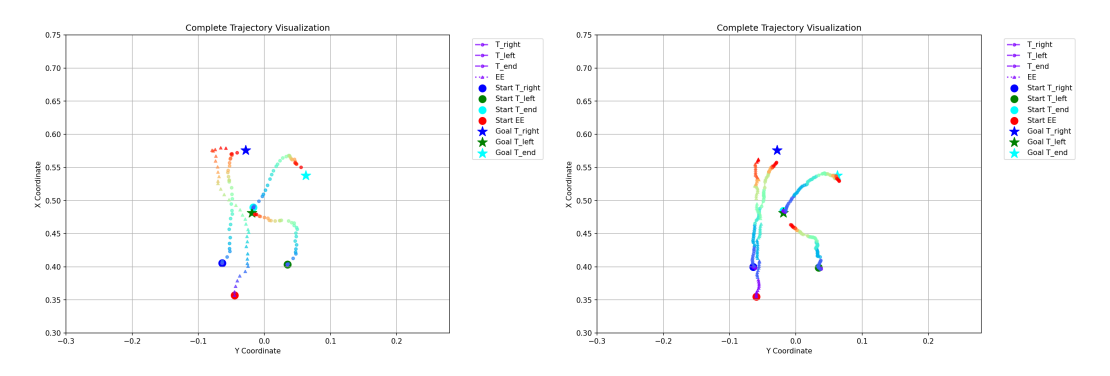


Figure 21: Trajectory of rotating T-block. Left: MPC_k^1 . Right: MPC_{AR} . Different colors represent controls from different plans.

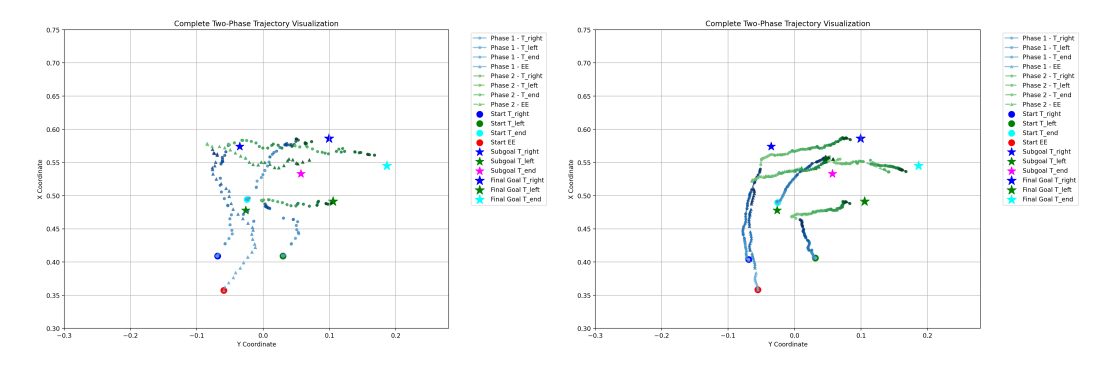


Figure 22: Trajectory of translating and rotating T-block. Left: MPC_k^1 . Right: MPC_{AR} . Different colors represent controls from different plans.



Figure 23: Visual demonstration for opening door to 90°.



Figure 24: Visual demonstration for opening door to 180° .



Figure 25: Visual demonstration for translating T-block.



Figure 26: Visual demonstration for rotating T-block.



Figure 27: Visual demonstration for translating and rotating T-block.

This small upfront investment unlocks the key benefits of our method: significant NFE reductions at runtime, robust performance across diverse tasks without re-tuning, and the ability to adapt to changing dynamics within a single episode. We believe this favorable trade-off is a core strength of our approach.

H LIMITATIONS

 Despite these promising results, this work has several limitations. A key challenge is the performance dependency on the quality of sensory input, particularly for vision-based models. As noted, future work should focus on developing more robust visual features, as the current approach's effectiveness can be hampered by visual corruptions or less discriminative features, leading to a performance gap compared to state-based world models where ADAREP excels. The current adaptive mechanism, while training-free and broadly applicable, relies on heuristic-driven parameter adjustments based on online estimates; the accuracy and reliability of these estimates are crucial, and noisy estimates could lead to suboptimal replanning decisions.

Future work should therefore focus on developing more robust visual features for vision-based models to broaden ADAREP's applicability. Additionally, exploring the integration of learning-based methods to further refine the adaptive parameters of ADAREP presents another promising research avenue, potentially leading to enhanced generalization and finer-grained adaptation across a wider array of tasks and conditions.